Long et al. J Infrastruct Preserv Resil (2022) 3:4
https://doi.org/10.1186/s43065-022-00049-2

Journal of Infrastructure Preservation and Resilience

RESEARCH

Open Access

Atomistic-scale investigation of self-healing mechanism in Nano-silica modified asphalt through molecular dynamics simulation

Zhengwu Long[1], Xianqiong Tang[2], Nanning Guo[1], Yanhuai Ding[2], Wenbo Ma[2], Lingyun You[1*] and Fu Xu[2*]

Abstract

As one of the most widely used nanomaterials in asphalt modification, the nano-silica (nano-SiO_2) can significantly improve the self-healing behavior of asphalt eco-friendly. However, understanding of the self-healing mechanism of nano-SiO_2 in asphalt is still limited. The objective of the study is to reveal the self-healing mechanism of nano-SiO_2 in asphalt by using molecular dynamics (MD) simulations from the nanoscale. A 10 Å (Å) vacuum pad was added between the two same stable asphalt models to represent the micro-cracks inside the asphalt. The self-healing process of virgin asphalt, oxidation aging asphalt, and nano-SiO_2 modified asphalt was studied using density evolution, relative concentration, diffusion coefficient, activation energy, and pre-exponential factor. The simulation results conclude that nano-SiO_2 improves the self-healing ability of asphalt by increasing the diffusion rate of molecules with aromatic structures without alkyl side chains and molecules with structures with longer alkyl chains. The self-healing capability of asphalt may be principally determined by the diffusion of light components such as saturate, while nano-SiO_2 only plays an inducing role. The research findings could provide insights to understand the self-healing mechanism of nano-SiO_2 in asphalt for promoting the sustainability of bitumen pavements while increasing their durability.

Keywords: Asphalt binder, Molecular dynamics, Self-healing mechanism, Nano-silica (SiO_2), Diffusion coefficient, Activation energy

*Correspondence: lingyunyou@hust.edu.cn; xufu@xtu.edu.cn
[1] School of Civil and Hydraulic Engineering, Huazhong University of Science and Technology, Wuhan 430074, Hubei Province, China
[2] College of Civil Engineering and Mechanics, Xiangtan University, Xiangtan 411105, Hunan Province, China

Graphical abstract

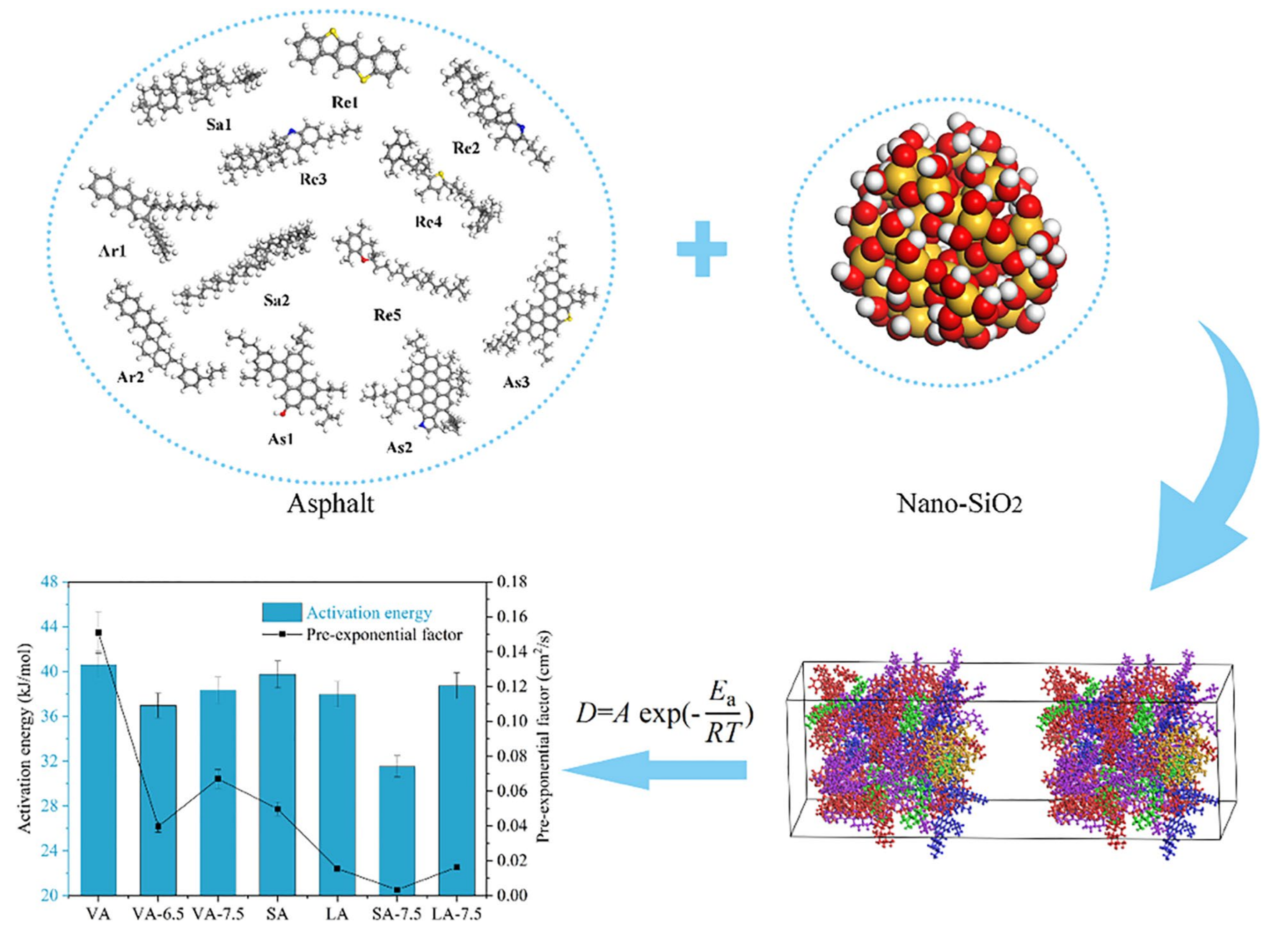

Background and introduction

Asphalt concrete is a composite material commonly used to surface roads, parking lots, and airports [1]. Asphalt mixtures have been used in pavement construction since the beginning of the twentieth century [2–4]. Although asphalt materials have typically used in pavement constructions, it has some defects such as low-temperature cracking and fatigue; thus, improving its self-healing performance is a critical way to solve this problem [5]. Proverbially, additive modification is also an excellent way to improve asphalt performance [6].

Due to some unique features of nanomaterials, such as high surface area, more and more researchers use nanomaterials to modify asphalt [7]. The application of nanoscale aluminum oxide (nano-Al_2O_3) in the virgin asphalt significantly improved the complex shear modulus. Nano-Al_2O_3 modification improved the high-temperature rutting resistance and low-temperature fatigue cracking resistance of asphalt [8]. The graphene was also used to enhance the high-temperature rutting resistance of asphalt [9, 10]. The carbon nanotube (CNT) can improve the ability to resist moisture damage in asphalt [11]. The hybrid CNTsgraphite powders can further enhance the mechanical properties of asphalt binders [12]. Noteworthy, the nano-silica (nano-SiO_2) modification presented an excellent global performance than other nanomaterials [13, 14], such as zero-valent iron and nano-clay [15]. Moreover, the previous studies found that the addition of nano-SiO_2 can remarkably enhance the properties of asphalt such as the resistances to oxidation aging [16], moisture damage [17, 18], and fatigue cracking [19].

Nowadays, many studies experimentally evaluate the effects of nanomaterials such as nano-graphene [20], nano-zycotherm [21], and nano-SiO_2 [22–24] on the self-healing properties of asphalt. These studies have shown that the simultaneous addition of Forta fibers and nano-zycotherm has a significant effect on the self-healing capability of asphalt [21]. Nano-graphene plays an advantageous role in the self-healing process [20]. Notably, the addition of nano-SiO_2 can significantly improve the self-healing behavior of asphalt mixtures [22, 23]. Therefore, nanomaterials can effectively enhance the self-healing properties of asphalt materials to alleviate the low-temperature cracking problem of asphalt. Researching the self-healing behavior and mechanism of asphalt materials has important theoretical significance for promoting the sustainability and eco-friendly of bitumen pavements. However, it is seldom applied to investigate the effect of nanomaterials on the self-healing mechanism of asphalt. Compared with other modifiers, the nano-SiO_2 can not only significantly improve the self-healing properties of the asphalt binder, but also improve the anti-oxidation and aging properties, moisture damage, and fatigue cracking properties. Thus, it is essential to conduct more in-depth research on the analysis of the self-healing mechanism of nano-SiO_2 in asphalt.

The mechanism analysis of asphalt materials was mainly performed by various computational and experimental techniques, including quantum mechanics (QM) calculations [25–27], Monte Carlo (MC) [28], molecular dynamics (MD) [29, 30], dissipative particle dynamics [31], and analytical chemistry [32], etc. Nevertheless, the MD simulation was proved to act as a powerful tool to predict the performances of asphalt materials and reveal its modification mechanism from the nanoscale [33, 34]. Some studies simulated the performance of asphalt via the MD method, which primarily involved its thermodynamic properties [35–37], oxidative aging [38–40], modification [41–44], diffusion behavior [45–47], and interface behavior [48–50]. Our previous work also studied the effect of aggregate surface irregularity and seawater erosion on interfacial adhesion properties of nano-SiO_2 modified asphalt mixtures via the MD method [51]. These studies have found that the MD method bridges the gap between macro- and micro-scope behaviors. Thus, MD has become a relatively mature computational method for asphalt materials design and performance prediction. Moreover, the aforementioned research studies also exhibit that the mechanism analysis of asphalt materials with the MD method has become a research hotspot.

In addition, the MD method has been widely employed in asphalt materials to analyze the influences of crack width [52], Styrene-Butadiene-Styrene (SBS) modifier [53], healing agent [54, 55], system temperature [56],

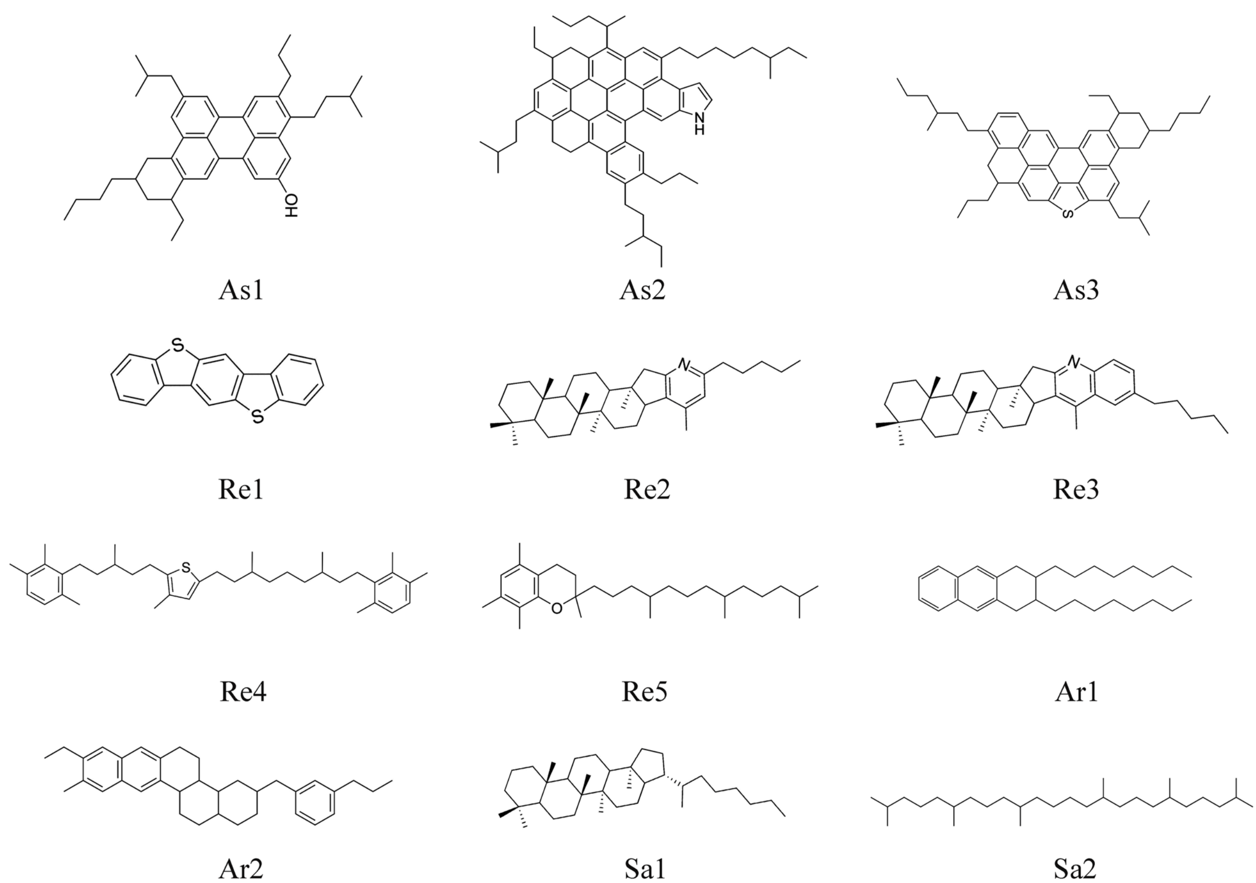

Fig. 1 12-Component Molecular Structures of Virgin Asphalt [62]

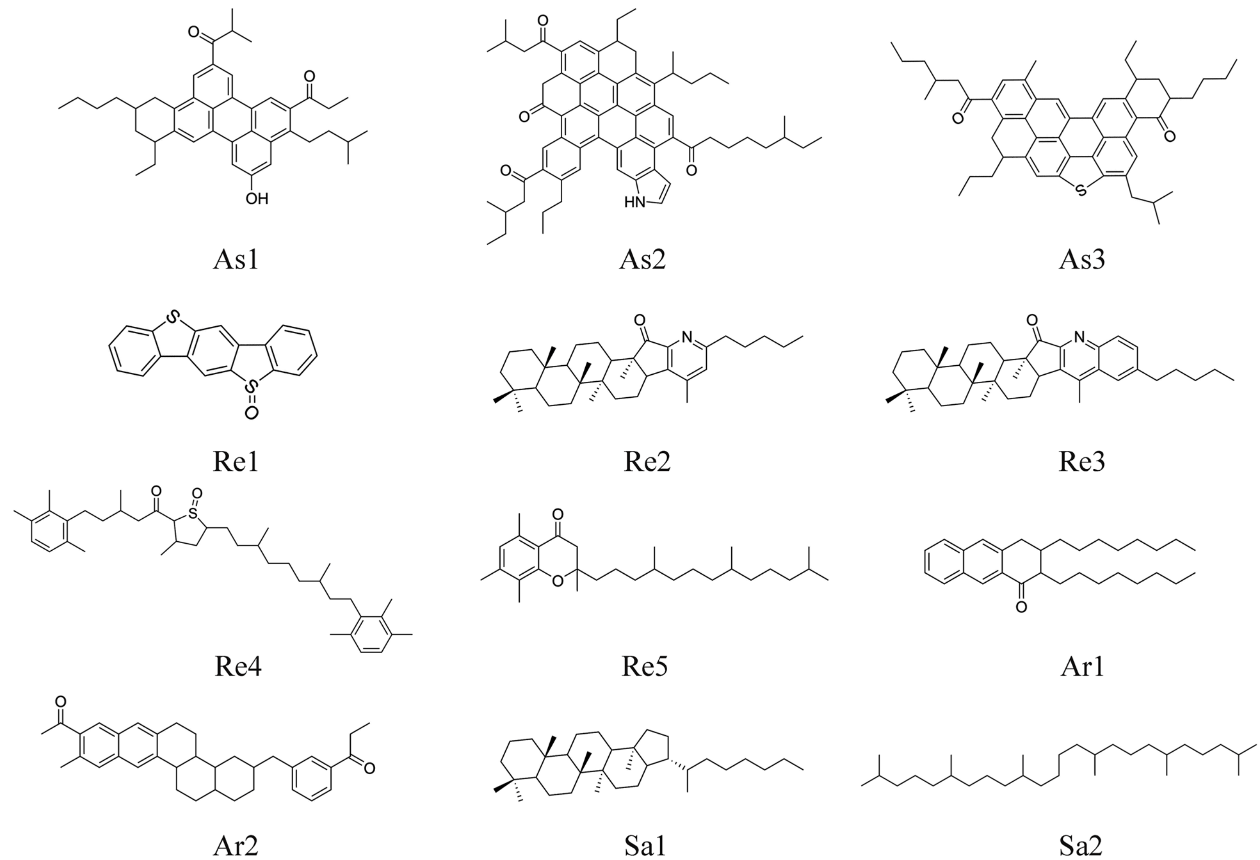

Fig. 2 12-Component Molecular Structures of Short-Term Aged Asphalt [63]

oxidation aging [39], and each component molecule [57] on the self-healing properties of asphalt. Moreover, a multi-gradient analysis of the self-healing behaviors of asphalt nano-cracks was carried out based on the MD method [58]. These studies have shown that the crack width has a more significant effect on self-healing than temperature, whereas oxidation aging harms the self-healing properties of asphalt. Therefore, it is critical to reveal the effect of nano-SiO_2 on the self-healing properties of asphalt to better understand the role of nano-silica in the self-healing behavior of asphalt and to further develop functional nano-SiO_2/polymer-asphalt composite system design from the nanoscale.

The primary objectives of the current study are to provide a comprehensive understanding of the effect of nano-SiO_2 on the self-healing properties of asphalt via MD simulations from the nanoscale. In this study, a vacuum pad was added between the two same stable asphalt models to represent the micro-cracks inside the asphalt. The asphalt model is verified by analyzing the density, viscosity, and glass transition temperature. The effect of nano-SiO_2 on the self-healing process was studied using density evolution, relative concentration, diffusion coefficient, activation energy, and pre-exponential factor.

Simulation models and methods

Force field and simulation details

The MD simulations were performed using Forcite-package of the Materials Studio 2017 software with the COMPASS, i.e., Condensed-Phase Optimized Molecular Potentials for Atomistic Simulation Studies, force field. The COMPASS force field is a first **ab initio** force field to make accurate predictions of materials properties for a wide range of compounds in isolation and condensed phases [59]. In the following all-atom MD simulation, the Lennard-Jones interactions and the Coulombic interactions were calculated with a cutoff radius of 12 Å. All the simulations were performed with a Nosé-Hoover thermostat and barostat [60, 61], and the time step was set to 1.0 fs. The conjugate gradients method was used for energy optimization, while the long-range interactions were measured with the particle-particle-particle-mesh (PPPM) algorithm.

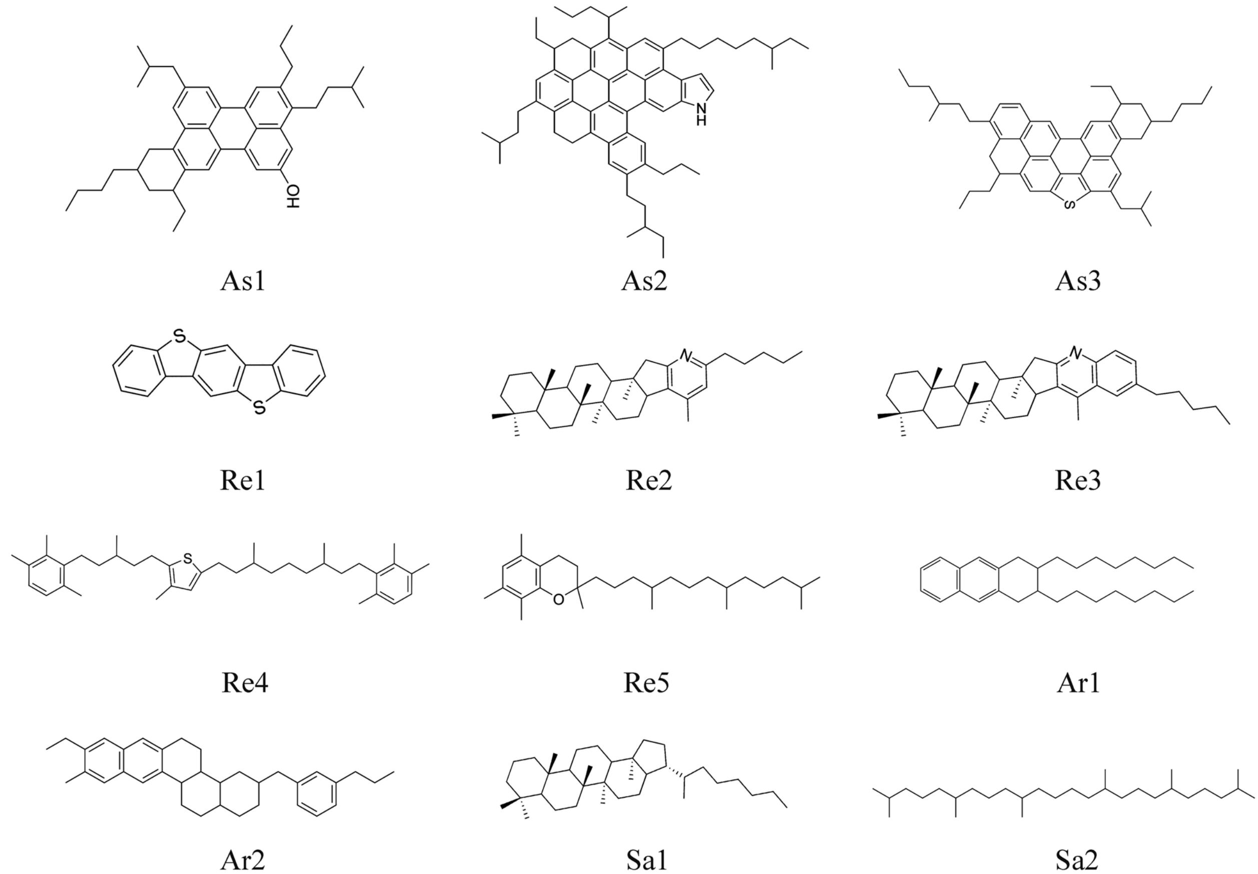

Fig. 3 12-Component Molecular Structures of Long-Term Aged Asphalt [39]

The asphalt is divided into SARA components, namely saturate (S), aromatic (A), resin (R), and asphaltene (A). To further understand the physical, rheological, and mechanical properties of asphalt, and improved 12-component asphalt model was proposed by Li and Greenfield [62] to represent the AAA-1, AAK-1, and AAM-1 asphalt. In this study, the proposed amorphous cell model for AAA-1 asphalt of the Strategic Highway Research Program was adopted to represent the original virgin asphalt. The molecular formulas of 12 kinds of molecules are shown in Fig. 1. The oxygen atom will quickly replace the hydrogen atom connected to the benzyl carbon atom in the asphalt molecule, and the sulfur atom in the sulfide can easily combine with the oxygen atom to form two main oxidizing functional groups: ketone and sulfoxide. Due to the lack of sensitive polar functional groups, the saturate molecules will not change after oxidative aging. The molecular polarity of other components will increase after the oxidative aging process of asphalt occurs. Therefore, the current method of establishing an aging asphalt model is mainly by changing the functional groups of the polar components (such as asphaltenes, resins, and aromatics) in the virgin asphalt. As the oxidation aging level of asphalt increases, the number of oxidized functional groups of each polar component will increase accordingly. The short-term aged and long-term aged asphalt molecular models proposed by Qu et al. [63] are used in this work. Figures 2 and 3 show the molecular models of short-term aged and long-term aged asphalt used in this study, respectively. The compositions of three asphalt models are demonstrated in Table 1.

A unit crystalline silica, with lattice parameters of $a = b = 4.913\,\text{Å}$, $c = 5.4052\,\text{Å}$, $\alpha = \beta = 90°$, and $\gamma = 120°$, was adopted from the Cambridge Structural Database. The sphere shape silica nanoparticle was built, and the radius of nano-SiO_2 was set as 5 Å, 5.5 Å, 6 Å, 6.5 Å, 7 Å, and 7.5 Å. The unsaturated boundary effect was eliminated by 1) adding hydrogen atoms to the unsaturated oxygen atoms and 2) adding hydroxyl groups to the unsaturated silicon atoms of the silica particle surface. Figure 4 shows the final nano-SiO_2 molecular model with a 7.5 Å radius.

To build the virgin and nano-SiO_2 modified asphalt model with different aging states, the assigned numbers

Table 1 Mass Percentage and Molecular Number of Virgin, Short-Term Aged, and Long-Term Aged Asphalt [51]

Fraction	Molecular	Label	Number in model	Virgin asphalt			Short-term aged asphalt		Long-term aged asphalt	
				Chemical formula	Mass fraction	Experimental data [64]	Chemical formula	Mass fraction	Chemical formula	Mass fraction
Saturate	Hopane	Sa1	4	$C_{35}H_{62}$	10.7	10.6	$C_{35}H_{62}$	10.3	$C_{35}H_{62}$	10.0
	Squalene	Sa2	4	$C_{30}H_{62}$			$C_{30}H_{62}$		$C_{30}H_{62}$	
Aromatic	DOCHN	Ar1	13	$C_{30}H_{46}$	30.8	31.8	$C_{30}H_{44}O$	31.0	$C_{30}H_{42}O_2$	31.5
	PHPN	Ar2	11	$C_{35}H_{44}$			$C_{35}H_{40}O_2$		$C_{35}H_{36}O_4$	
Resin	Benzobisbenzothiophene	Re1	5	$C_{18}H_{10}S_2$	41.9	37.3	$C_{18}H_{10}OS_2$	41.9	$C_{18}H_{10}O_2S_2$	41.4
	Pyridinohopane	Re2	4	$C_{36}H_{57}N$			$C_{36}H_{55}NO$		$C_{36}H_{53}NO_2$	
	Quinolinohopane	Re3	4	$C_{40}H_{59}N$			$C_{40}H_{57}NO$		$C_{40}H_{55}NO_2$	
	Thioisorenieratane	Re4	4	$C_{40}H_{60}S$			$C_{40}H_{58}O_2S$		$C_{40}H_{56}O_3S$	
	Trimethylbenzeneoxane	Re5	15	$C_{29}H_{50}O$			$C_{29}H_{48}O_2$		$C_{29}H_{48}O_2$	
Asphaltene	Asphaltene-phenol	As1	3	$C_{42}H_{54}O$	16.6	16.2	$C_{42}H_{50}O_3$	16.8	$C_{42}H_{46}O_5$	17.1
	Asphaltene-pyrrole	As2	2	$C_{66}H_{81}N$			$C_{66}H_{73}NO_4$		$C_{66}H_{67}NO_7$	
	Asphaltene-thiophene	As3	3	$C_{51}H_{62}S$			$C_{51}H_{58}O_2S$		$C_{51}H_{54}O_5S$	

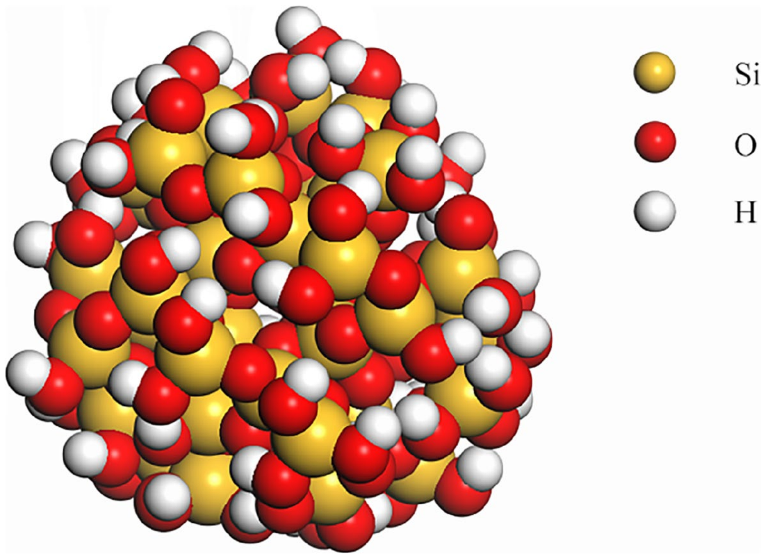

Fig. 4 Nano-SiO_2 Clusters in the Models

of each type of molecule were filled into a cubic box with an initial density of 0.8 g/cm^3 to randomly distribute all molecules and prevent the molecule chains twisting with each other. Three different initial configurations were created at each temperature to average over different initial mixing of the components. After an energy optimization progress, all asphalt models were equilibrated in the canonical ensemble (NVT) at 298 K for 5 ns. After NVT, an isothermal-isobaric ensemble (NPT) of 20 ns at one atmosphere was followed to ensure system equilibration for further data analysis. The temperatures were selected at 298 K, 333 K, 368 K, 403 K, 438 K, and 473 K.

Self-healing models

After determining the equilibrated asphalt MD model, a 10 Å vacuum pad was added between the two same stable models to represent the micro-cracks inside the asphalt. The diffusion between the two asphalt layers can emulate the self-healing process. The NPT ensemble was adopted for the first 2 ns at 1 atm. During this time, the asphalt layers exhibit a short self-balancing at the beginning of the self-healing process. The relative concentration curves in the z-direction were collected during the NPT ensemble simulation. After end of the NPT ensemble simulation, the NVT ensemble simulation was used further for another 20 ns at five different temperatures to simulate the molecular diffusion across the healing micro-crack surface. The simulation temperatures were set within 298–438 K, including 298 K, 333 K, 368 K, 403 K, and 438 K. The 3D micro-crack model of virgin asphalt is demonstrated in Fig. 5 (a).

MD simulation theories and methods

(1) **Viscosity:** Viscosity is a measure of the resistance of fluid flow. This study performed a non-equilibrium molecular dynamics (NEMD) simulation [65] by shearing the simulation box and applied SLLOD equations of motion [66] to calculate viscosity. Figure 6 shows the initial and shearing simulation box during the viscosity simulation. This research used the NVT ensemble to perform the viscosity simulations for 60 ns. In addition, three different constant shear rates ($\times 10^{10}$, 10^9, and 10^8 /s) were used to deform the simulation box.

(2) **Glass transition temperature:** The glass transition temperature is a significant parameter in determining the viscoelastic properties of asphalt. The glass transition is a reversible process from a hard or brittle glassy state to a molten or rubber-like viscoelastic state. The glass transition temperature refers to the temperature corresponding to the transition from a fragile glassy state to a viscoelastic state. During the glass transition, the physical properties such as specific volume will change massively. In this work, all equilibrium asphalt models were initially heated up to a temperature of 600 K and were subjected to stepwise cooling at a rate of 5 K/ns (temperature was reduced in steps of 10 K per 2 ns) until a low temperature of 80 K was reached. The specific volume of the systems was determined by averaging its values over the second half of the 2 ns

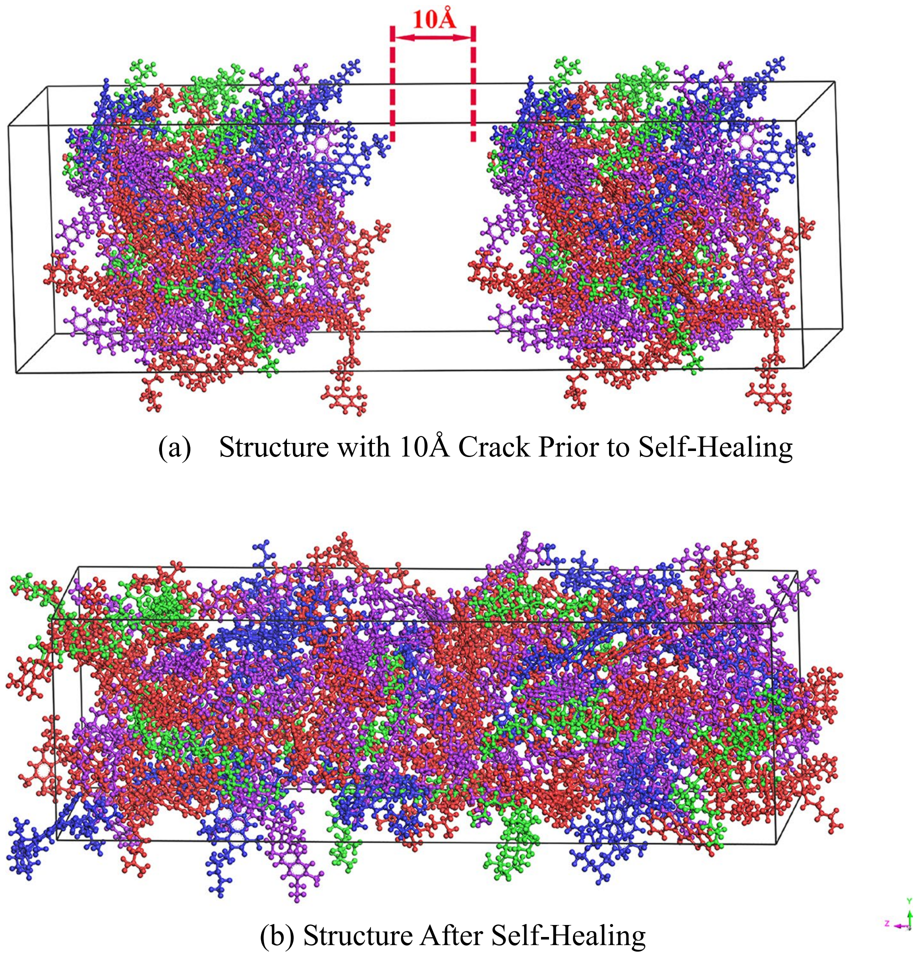

Fig. 5 Self-Healing Process in the Virgin Asphalt Model: (**a**) Structure with 10 Å Crack Prior to Self-Healing and (**b**) Structure After Self-Healing (asphaltene, resin, aromatic, and saturate are represented as blue, purple, red, and green, respectively)

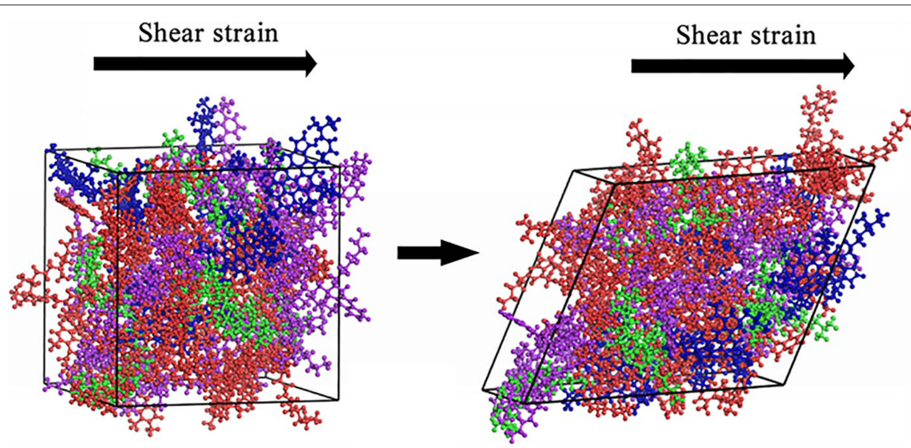

Fig. 6 MD Simulation Box with Initial and Shearing Conditions for Viscosity Calculations (asphaltene, resin, aromatic, and saturate are represented as blue, purple, red, and green, respectively)

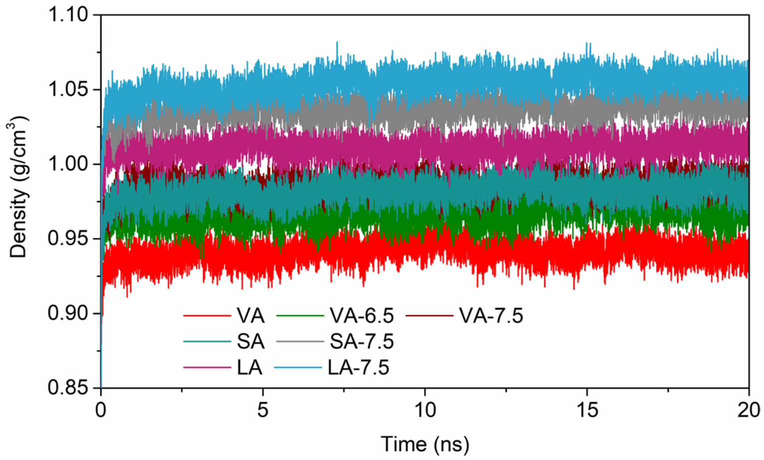

Fig. 7 Density Curves of the Asphalt Models at 333 K during 20 ns All-Atom MD Simulations. It shall be noted that VA is for virgin asphalt, SA is for short-term aged asphalt, and LA is for long-term aged asphalt. The number with the labels indicates the corresponding nano-SiO_2 modified asphalt and the size of the number is the radius of the nano-SiO_2 particles with the unit of Å

long run at each cooling step. The glass transition temperature was defined as the intersection of two fitting lines in the brittle glass-like and viscoelastic rubber-like regions of the specific volume versus temperature curve [67].

(3) **Self-healing:** The mean square displacement (MSD) of the molecules tracks the translational mobility of asphalt molecules. The diffusion coefficient is related to the MSD as a function of time, as shown in Eq. (1). The diffusion coefficient is temperature-dependent and can be expressed by Arrhenius law, as shown in Eq. (2) [68].

$$D = \frac{a}{2d} \tag{1}$$

$$D = A\ \exp\left(-\frac{E_a}{RT}\right) \tag{2}$$

or what it is the same as

$$\ln(D) = \ln(A) - \frac{E_a}{R}.\frac{1}{T} \tag{3}$$

where D is diffusion coefficient; a is the slope of the straight line fitted by the MSD curve with time (the unit of a is $10^{-4}\,cm^2/s$); d is the system dimensionality, and in this work $d=3$; A is the pre-exponential factor; E_a is the activation energy of the system; R is the molar gas constant (8.314 J/mol/K); T is the temperature of the system.

The activation energy and pre-exponential factor are two critical parameters for evaluating the self-healing behavior of asphalt. The activation energy can be regarded as the energy required for the asphalt self-healing process initialization. The pre-exponential factor is related to the instantaneous self-healing ability of the asphalt (the more significant the value, the stronger the instantaneous healing ability).

Simulation results and discussion

Thermodynamic properties and model validation

The thermodynamic properties of asphalt models were calculated to ensure the accuracy of the MD method and asphalt molecule models, including density, viscosity, and glass transition temperature. The density values of seven different asphalt molecules models are shown in Fig. 7. The consistent fluctuation of instantaneous density around the average density with simulation time was observed to show that the asphalt systems reached stable status. The average density values at different temperatures were calculated, as shown in Fig. 8. The highest predicted density is 1.06 g/cm^3 at 298 K, and the densities reduce to 0.85 g/cm^3 at 473 K. The density of all asphalt models ranges from 0.94 to 1.05 g/cm^3 at 333 K slightly lower than experiment data from 0.99 to 1.33 g/cm^3 at 333 K [69]. This is rational because the evaporation of saturates in the aging process was not considered in the simulation process.

Figure 9(a) shows the viscosity values for six different bulk asphalt model at 333 K at the different shear rates. The reducing simulation viscosity values for higher shear rates indicate that the asphalt models exhibit shear-thinning behavior at high shear rates. Figure 9(b) presents the viscosity values for six different bulk asphalt models at 10^8/s shear rate at the five three different temperatures.

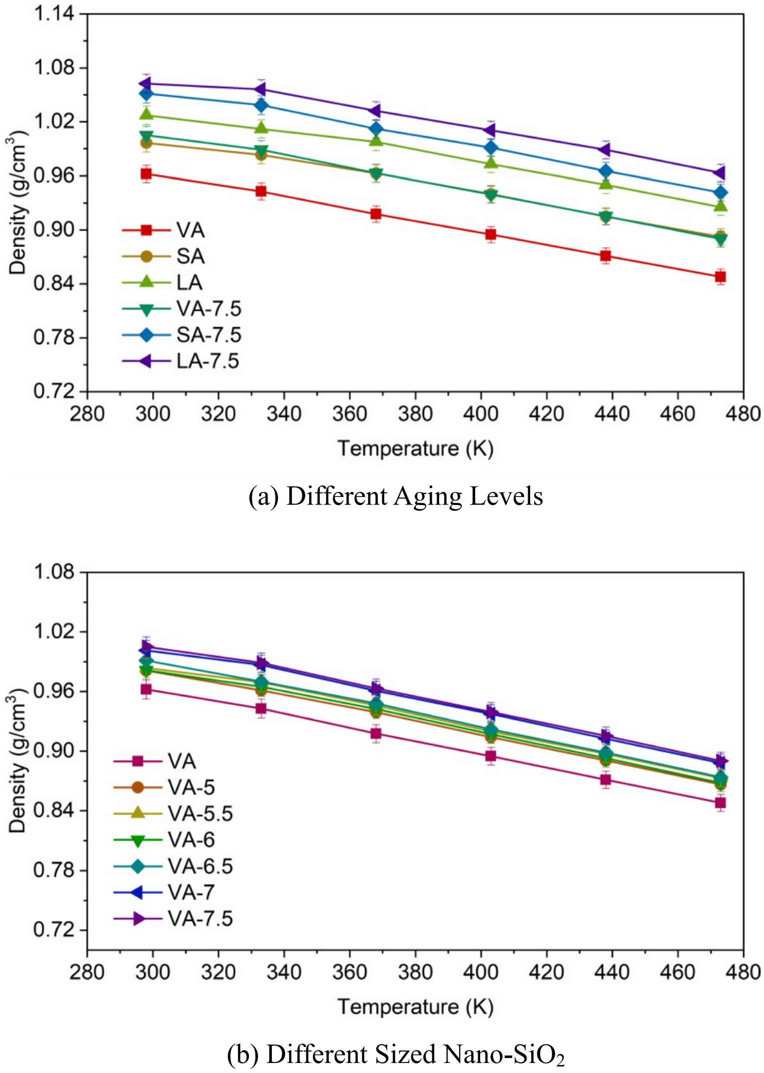

Fig. 8 Density of Asphalt Models at Different Aging Level and with Different Sized Nano-SiO_2 on during 20 ns All-Atom MD Simulations: (**a**) Different Aging Levels, and (**b**) Different Sized Nano-SiO_2

The stable viscosity value of the virgin asphalt model at 10^8/s shear rate at 403 K was around 12.96 cP, close to Kim's simulation results from 7.32 to 13.9 cP at 10^8/s shear rate at 408 K [40].

Figure 10 provides the relationship between specific volume and temperature for the AAA-1 virgin asphalt model. In general, the specific volume increases with the increase in temperatures, and the rate of growth in the high-temperature zone is significantly higher than in the low-temperature region. There exists a visible glass transition zone between the high-temperature zone and the low-temperature zone. The glass transition temperature of the virgin asphalt model is around 266 K. It shows good agreement with literature reported experimental data from 223 K to 303 K [70]. The glass transition temperature results of six different asphalt models are presented in Fig. 11. As shown, the glass transition temperature increases as the asphalt become stiff due to oxidation aging. This finding is consistent with previous reports in the literature [71]. And the glass transition temperature of nano-SiO_2 modified asphalt is higher than the unmodified asphalt. This is because the nano-SiO_2 can enhance the high-temperature property of asphalt materials [7].

The relationship between the energy component and temperature of the AAA-1 virgin asphalt model

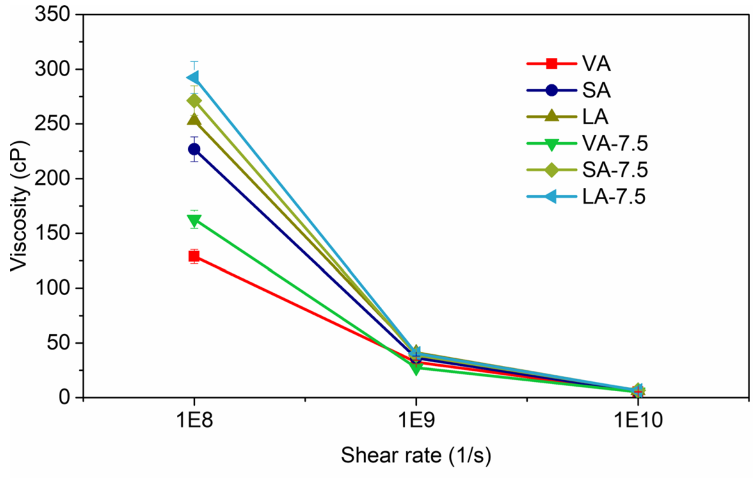

(a) Different Shear Rates

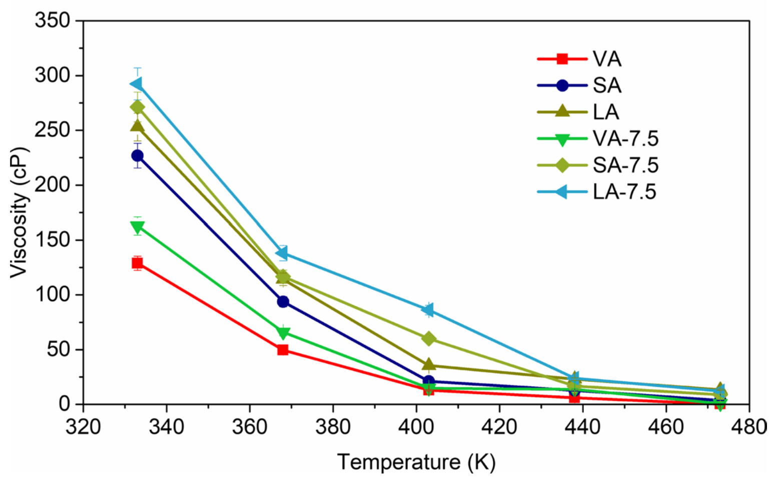

(b) Different Temperatures

Fig. 9 Viscosity of Asphalt Models at Different Aging Levels during 60 ns All-Atom MD Simulations: (**a**) Different Shear Rates, and (**b**) Different Temperatures

is shown in Fig. 12. The relationship between intra-molecular energy and temperature is almost a straight line. Conversely, a glass transition region appears in the intermolecular energy (van der Waals energy and electrostatic energy) versus temperature curve. This means that from an energy perspective, with the change of temperature, the generation of glass transition behavior is mainly related to the intermolecular energy.

According to the above analysis, the MD simulations results are similar to previous study results based on the real asphalt in the laboratories. Therefore, it is reasonable that the simulation method and the asphalt molecule model can predict the properties of asphalt accurately.

Influence of nano-SiO_2 on the self-healing potential of asphalt

Density and relative concentration in the self-healing process

Virgin asphalt molecules diffuse across the nano-crack, and the vacuum layer inside the model gradually disappears. The layer structure after the self-healing is demonstrated in Fig. 5(b). The density evolution with the self-healing process is shown in Fig. 13. As shown, the density of all models begins to enter a stable state at 0.5 ns. The self-healing asphalt recovers to the same density as the original asphalt compared with Fig. 7. The self-healing process of asphalt nano-crack is divided into two parts in Fig. 13. The first stage (0–0.5 ns), the typical artificial nano-crack healing stage, was where an asphalt

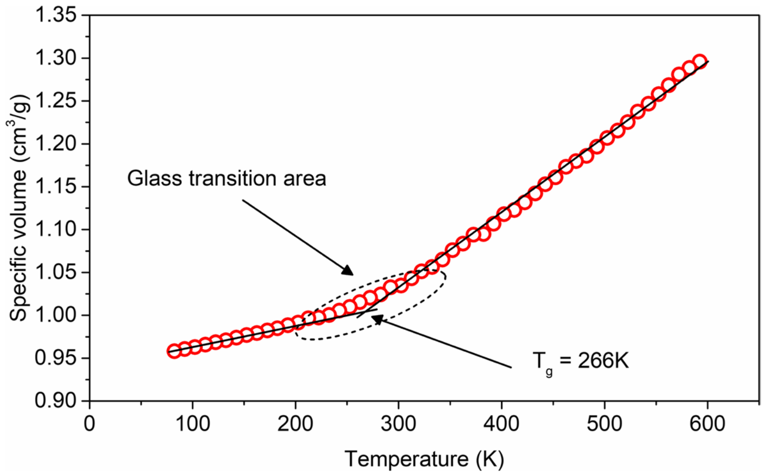

Fig. 10 Specific Volume versus Temperature Diagrams for Virgin Asphalt Model at the Temperatures from 80 to 600 K

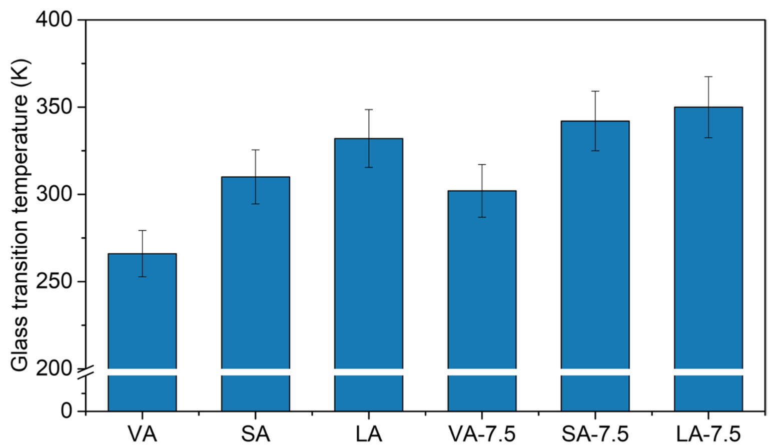

Fig. 11 Glass Transition Temperature of the Asphalt Models

layer and another asphalt layer moved closer together until the vacuum layer disappeared. The self-healing model density value increases rapidly and then gradually increases until the final mutation approaches the original model density value. However, the density change between 0 and 0.5 ns did not show an obvious rule. This is because the initial self-healing model is not stable, resulting in relatively large energy fluctuations in the initial model. The second stage (0.5–2 ns), the actual self-healing stage, was characterized by a stable density curve and close to the original asphalt density.

The relative concentrations of asphalt molecules in the *z*-direction are calculated to study the self-healing behavior. The relative concentration distribution of the virgin asphalt 3D nano-crack model in the *z*-direction at 298 K is shown in Fig. 14. At 0 ps, the relative concentration of the asphalt model showed a bimodal distribution. The relative concentration at the middle and the edges were both 0.0, indicating that the asphalt has not started to heal. From 200 ps to 400 ps, the relative concentration of the two peaks decreased significantly. The relative concentration of the middle valley began to increase, and the crack width gradually decreased, indicating that the asphalt molecules began to diffuse toward the middle crack. From 600 ps to 1000 ps, both peaks and valleys disappear, and the relative concentration approaches 1.0, the molecules on both sides of the crack come into contact, and the asphalt molecular model begins to heal. This finding is consistent with changes in density.

As shown in Fig. 15, the relative concentration values were close to 0 in the nano-crack area of the *z*-direction before healing. As the temperature rises, the two peaks

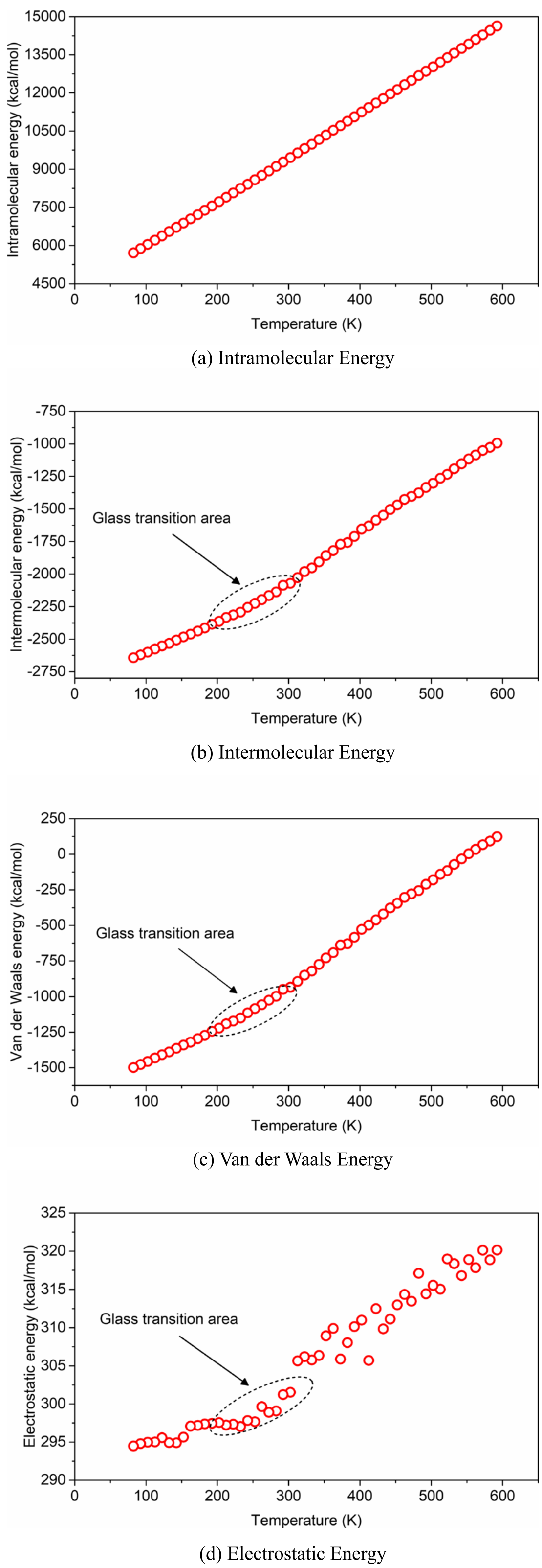

Fig. 12 Model Energies versus Temperature Diagrams for the Asphalt Models at the Temperatures from 80 to 600 K: (**a**) Intramolecular Energy, (**b**) Intermolecular Energy, (**c**) Van der Waals Energy, and (**d**) Electrostatic Energy

decrease, and the width of the artificial crack in the middle gradually decreases. When the temperature rises to 368 K, the valley is invisible, and the relative concentration values along the entire length were close to 1.0, indicating that the artificial cracks have disappeared. This is because the increase in temperature will lead to increased molecular diffusion and accelerate the self-healing behavior of asphalt. Therefore, it is necessary to use the diffusion coefficient to analyze the self-healing behavior of asphalt.

Diffusion coefficient analysis in the self-healing process

Asphalt typically behaves as a Newtonian fluid above the glass transition temperature, and self-healing would occur [72]. Van der Waals forces are the main factor affecting the self-healing of asphalt [57]. It is found from Section 3.1 that the glass transition behavior is related to van der Waals interaction. This also means that there may be a special relationship between the glass transition behavior of asphalt self-healing behavior. Therefore, this paper mainly studies the diffusion rate above the glass transition temperature because this is the crucial factor affecting the self-healing behavior of asphalt.

The MSD curves of the seven asphalts at 298 K are shown in Fig. 16. As expected, the MSD increases with simulation time, and the slope of nano-SiO_2 modified virgin asphalt is slightly higher than that of virgin asphalt. The slope of aged asphalt is significantly lower than that of virgin asphalt. This means that the addition of nano-SiO_2 can promote the translation mobility of asphalt molecules. The oxidation aging of asphalt molecules is not conducive to the migration of asphalt molecules.

The diffusion coefficient of seven asphalt at 298 K and 333 K are shown in Fig. 17. It can be found that a higher temperature will facilitate the self-diffusion of asphalt molecules and promote healing capability. Overall, the diffusion coefficients of nano-SiO_2 modified asphalt are higher than the virgin asphalt, and oxidation aging asphalt have a lower diffusion coefficient than virgin asphalt. This conclusion is well consistent with past findings [39, 57]. The diffusion coefficient of VA-7.5 is the highest, followed by VA-6.5, VA, SA-7.5, SA, and LA, the diffusion coefficients of LA and LA-7.5 are similar. This means that nano-SiO_2 can enhance the self-healing ability of asphalt, while oxidative aging will reduce the

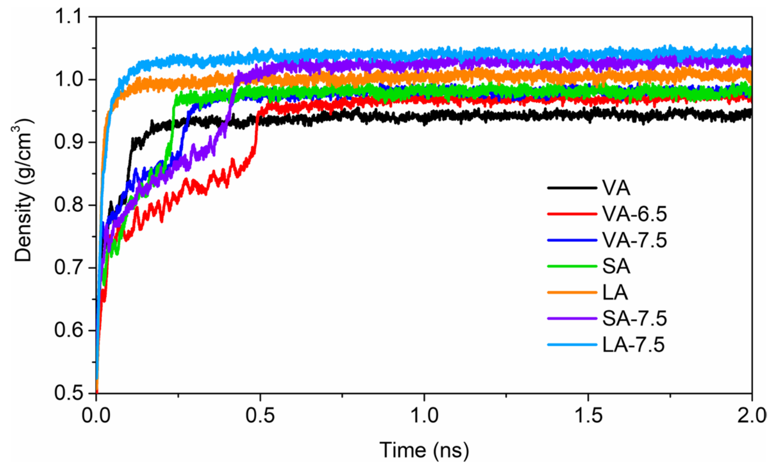

Fig. 13 Model Density Changes during Self-Healing Process at 333 K

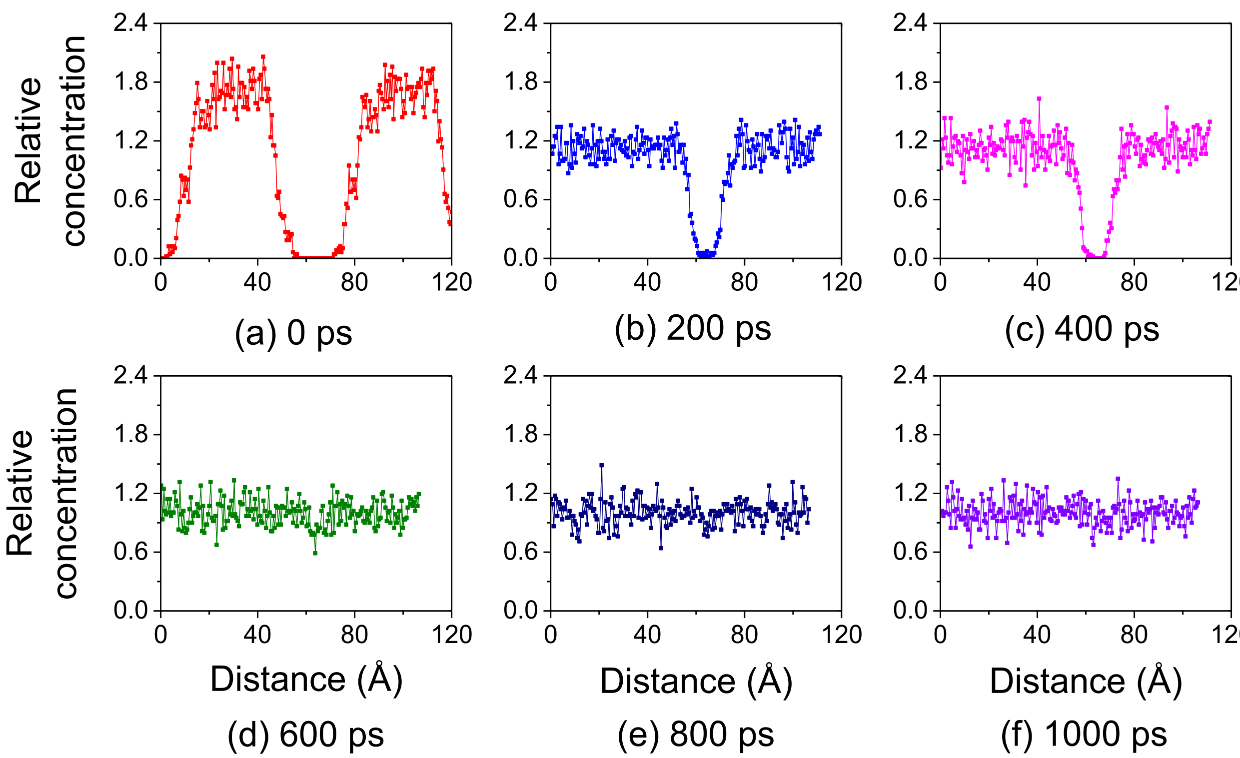

Fig. 14 Relative Concentration Distribution of Nano-Crack Model in the z-direction at 298 K at Difference Running Time (from 0 to 1000 ps)

self-healing capability of asphalt. In other words, the nano-SiO_2 additive has the effect of indirectly improving the ability to resist oxidation aging.

To further study the effect of nano-SiO_2 on self-healing behavior, the diffusion coefficients of 4-components of seven asphalt models at 333 K were calculated, as shown in Fig. 18. In general, the diffusion coefficient of asphaltene is lower than other 3-components (except nano-SiO_2) for all seven asphalt models. Figure 18(a) shows that the diffusion coefficient of the four-components generally increases after the addition of nano-SiO_2. Conversely, Fig. 18(b) shows that the diffusion coefficient of 4-components has a general downward trend as the degree of oxidation aging increases. For virgin asphalt,

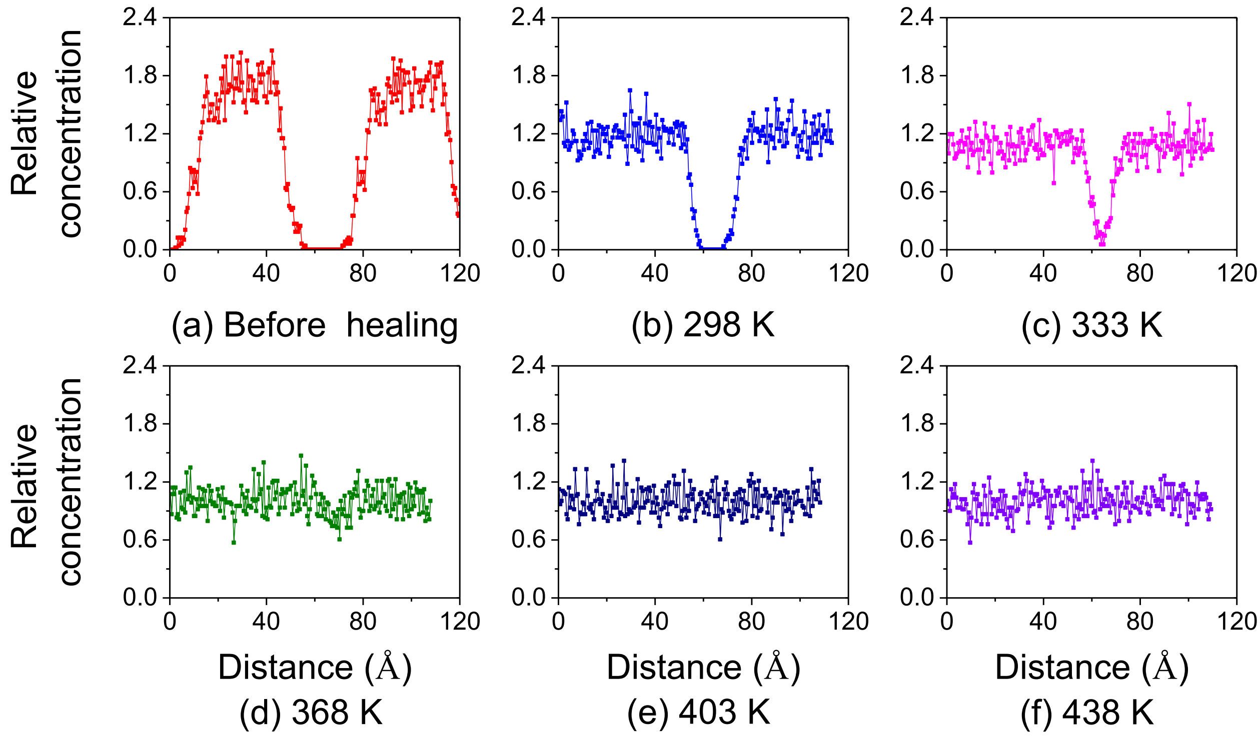

Fig. 15 Relative Concentration Distribution of Nano-Crack Model in the *z*-direction at 100 ps at Different Temperatures (from 298 to 438 K)

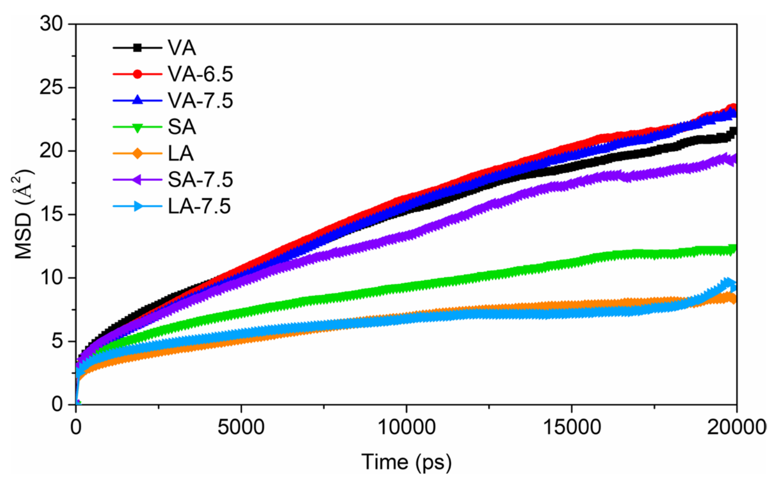

Fig. 16 MSD Curves of the Asphalt Models during Self-Healing Process at the Temperature of 298 K

the diffusion coefficients of saturate are the highest, followed by aromatic, resin, and asphaltene. This is related to asphalt 4-components molecular weight. In particular, with the addition of nano-SiO_2 modifier, the diffusion coefficient of asphaltene reduces compared to the virgin asphalt, whereas the diffusion coefficients of other 3-components increase obviously. This indicates that nano-SiO_2 has a significant enhancement effect on the diffusion rates of saturate, aromatic, and resin. Alternatively, the diffusion coefficient of nano-SiO_2 is low. In other words, the self-healing capability of asphalt may be mainly determined by the diffusion of light components such as saturate, while nano-SiO_2 only plays an inducing role.

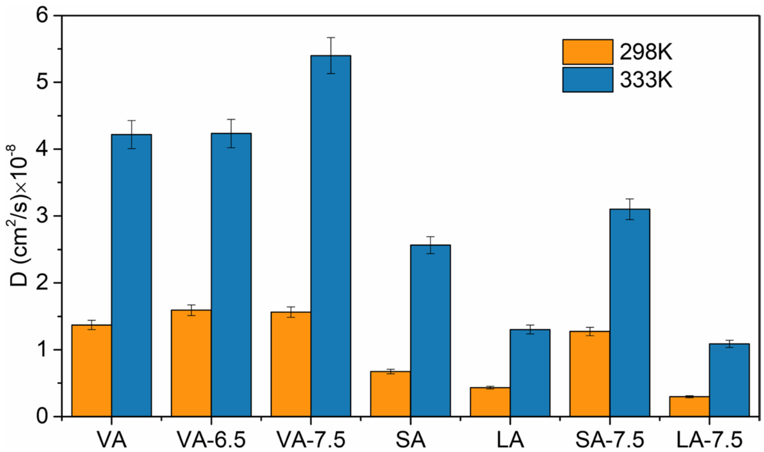

Fig. 17 Diffusion Coefficient of the Asphalt Models during Self-Healing Process at the Temperatures of 298 K and 333 K

The virgin asphalt molecular model established in this work consists of 12 different molecules. The diffusion rates of these 12 molecules are different. Researching the diffusion rate of all types of molecules is conducive to the selection of appropriate modifiers to precisely increase the molecular diffusion rate and enhance the self-healing capability of the asphalt. Figure 19 shows the comparison of 12 different molecules diffusion coefficient of the virgin asphalt, long-term aged asphalt, and nano-SiO_2 modified asphalt at 333 K. For three asphalt models, the molecule with the most significant diffusion coefficient is Re1, and the molecule with the lowest diffusion coefficient is As1 (except nano-SiO_2). The diffusion coefficient of all 12 molecules in the long-term aged asphalt model is lower than that of the virgin asphalt model. Specifically, among the virgin asphalt, the three molecules with the most significant diffusion coefficients are Ar1, Sa1, and Re1 in ascending order. For the long-term aged asphalt, the three molecules with the most significant diffusion coefficients are Re1, Ar1, and Sa2 in descending order. As for the nano-SiO_2 modified asphalt model, the three molecules with the most considerable diffusion coefficients are Re1, Sa2, and Re5 in descending order. However, the diffusion coefficient of the nano-SiO_2 modifier is the lowest among the other 12 molecules of nano-SiO_2 modified asphalt. Thus, molecules with aromatic structures without alkyl side chains (Re1) and molecules with structures with longer alkyl chains (Ar1, Sa2, Re5) may diffuse more easily; molecules with complex aromatic structures and more short alkyl side chains (As1) may be more difficult to diffuse. Nano-SiO_2 mainly improves the self-healing ability of the asphalt by enhancing the diffusion rate of molecules with aromatic structures without alkyl side chains and molecules with longer alkyl chains structures.

Activation energy analysis in the self-healing process

To further study the effect of nano-SiO_2 on the self-healing behavior of asphalt, the activation energy and pre-exponential factor of the self-healing process were calculated based on Arrhenius law. Figure 20 plots the relationship between logarithmic of diffusion coefficients and temperatures reciprocal for virgin asphalt, short-term aged asphalt, and long-term aged asphalt. As depicted in Fig. 20, the diffusion rate increases with an increase in the temperature for all three asphalts. As seen from the fitting equation in Table 2, E_a/R is a constant for all seven asphalts nano-crack models; that is, the logarithm of the diffusion coefficient is linearly correlated with the reciprocal of temperature. Figure 21 compares the activation energy and pre-exponential factor of seven different asphalt. The activation energy calculated for VA-6.5 and VA-7.5 is a little lower than that of VA, while the pre-exponential factor of VA is much more significant than VA-6.5 and VA-7.5. It indicates that nano-SiO_2 modified asphalt has a low activation energy barrier, although the instantaneous self-healing ability is weak. Simultaneously, nano-SiO_2 modified asphalt has a more significant diffusion coefficient, so it is believed that nano-SiO_2 can effectively improve the self-healing properties of asphalt as long as the temperature is higher than the glass transition temperature.

For three different oxidation aging state asphalt, the pre-exponential factor of VA is the highest, followed by SA and LA. This means that as the degree of oxidative aging of asphalt increases, the instantaneous self-healing ability of asphalt weakens. However, the changing trend of activation energy is consistent with the pre-exponential factor, which is inconsistent with previous literature reports [39]. This may be because in the aging model, only the oxidation of molecules is considered, and the

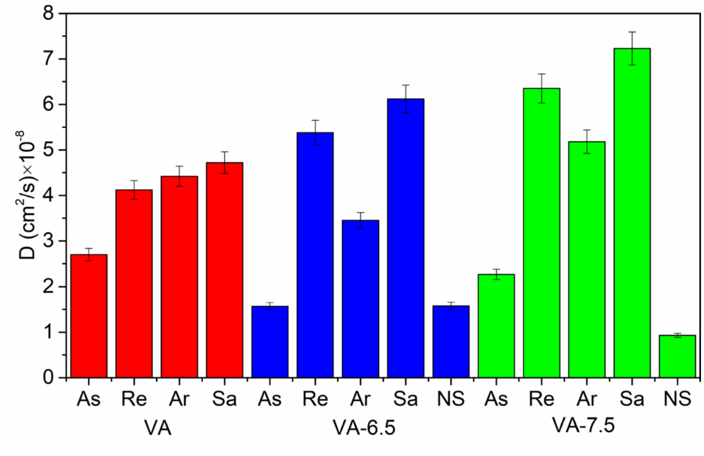

(a) VA, VA-6.5, and VA-7.5

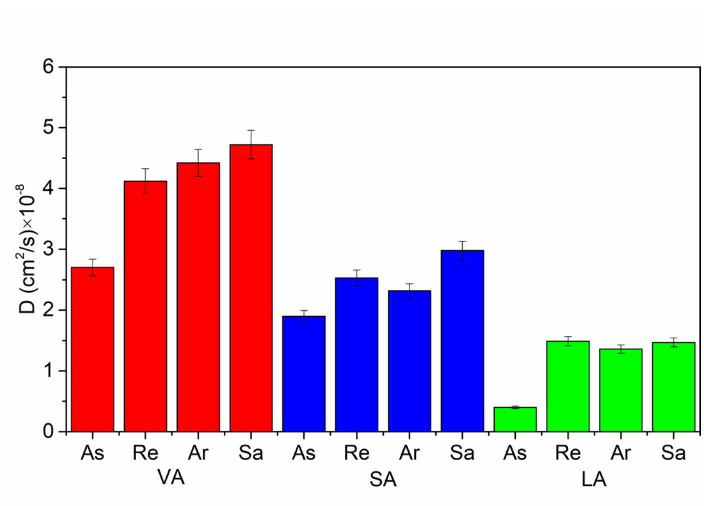

(b) VA, SA, and LA

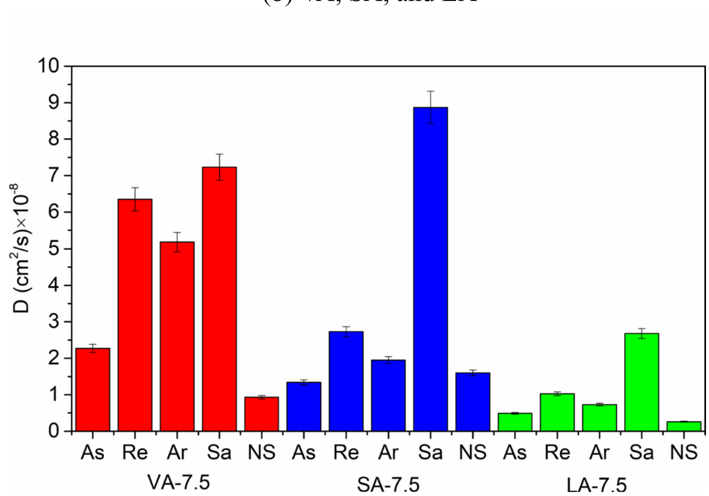

(c) VA-7.5, SA-7.5, and LA-7.5

Fig. 18 Comparison of the Molecular Diffusion Coefficient of the Components in the Asphalt Models at 333 K: (**a**) VA, VA-6.5, and VA-7.5, (**b**) VA, SA, and LA, and (**c**) VA-7.5, SA-7.5, and LA-7.5. It shall be noted that As is for asphaltene, Re is for resin, Ar is for aromatic, Sa is for saturate, and NS is for nano-SiO_2

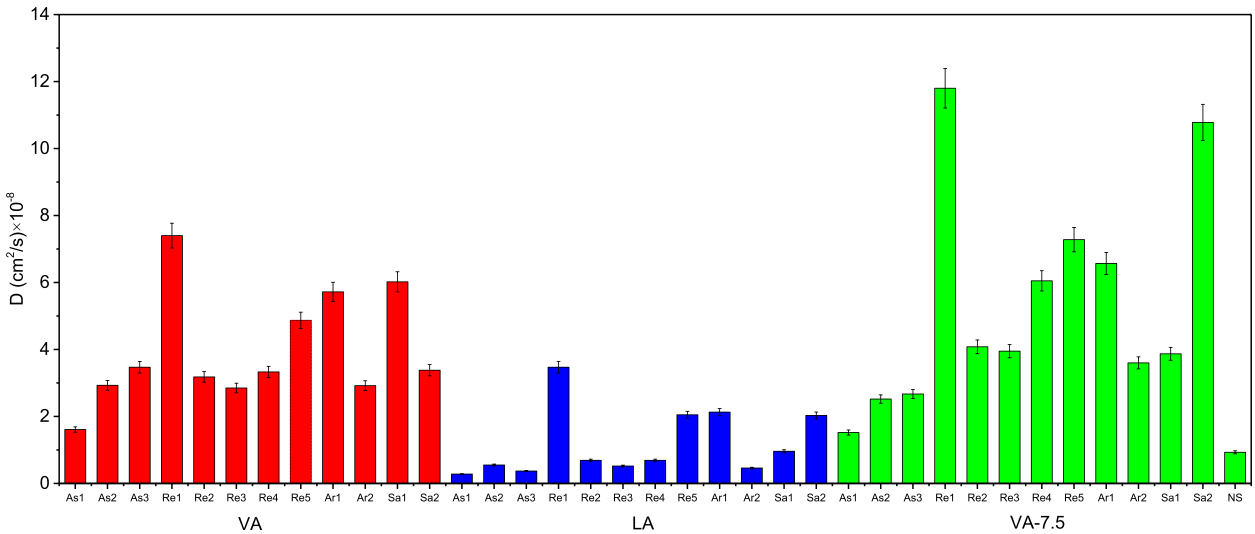

Fig. 19 Molecular Diffusion Coefficients of Virgin Asphalt, Long-Term Aged Asphalt, and nano-SiO_2 Modified Asphalt at 333 K. It shall be noted that As1 is for asphaltene-phenol, As2 is for asphaltene-pyrrole, As3 is for asphaltene-thiophene, Re1 is for benzobisbenzothiophene, Re2 is for pyridinohopane, Re3 is for quinolinohopane, Re4 is for thioisorenieratane, Re5 is for trimethylbenzeneoxane, Ar1 is for dioctyl-cyclohexane-naphthalene (DOCHN), Ar2 is for perhydrophenanthrene-naphthalene (PHPN), Sa1 is for hopane, and Sa2 is for squalane

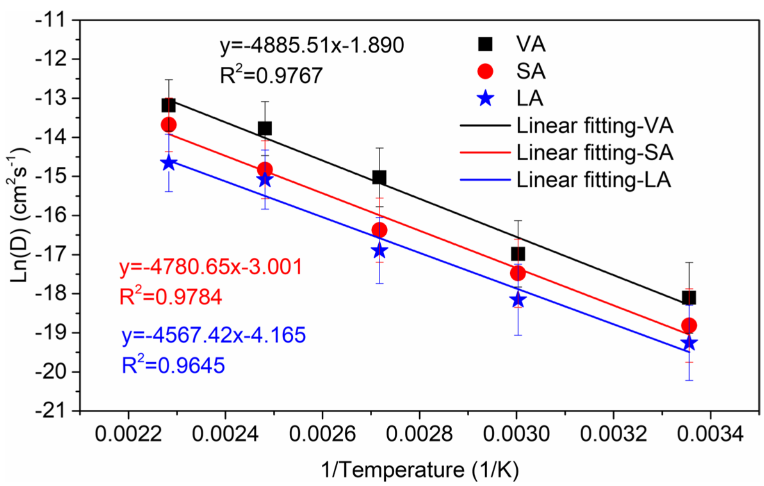

Fig. 20 Diffusion Coefficient versus Simulation Temperatures for Virgin Asphalt, Short-Term Aged Asphalt, and Long-Term Aged Asphalt

Table 2 Fitting Results of the Diffusion Coefficient versus System Temperature Base on Arrhenius Law

Models	Fitting formula of lnD and 1/T	R^2
VA	lnD = − 4885.51/T-1.890	0.9767
VA-6.5	lnD = − 4446.90/T-3.229	0.9799
VA-7.5	lnD = − 4612.30/T-2.703	0.9865
SA	lnD = − 4780.65/T-3.001	0.9784
LA	lnD = − 4567.42/T-4.165	0.9645
SA-7.5	lnD = − 3792.21/T-5.707	0.9626
LA-7.5	lnD = − 4660.09/T-4.117	0.9858

disturbance of SARA components is not considered. Therefore, the influence of oxidative aging on the self-healing properties of asphalt may require more in-depth research. Since LA has lower activation energy, healing is achieved faster in the initial stage of self-healing. This can also explain the healing time after short-term aging is longer than that of virgin asphalt, and the healing time after long-term aging is shorter than that of virgin asphalt (Fig. 13).

Moreover, comparing the activation energy and pre-exponential factor of VA-7.5, SA, and LA asphalt, it can

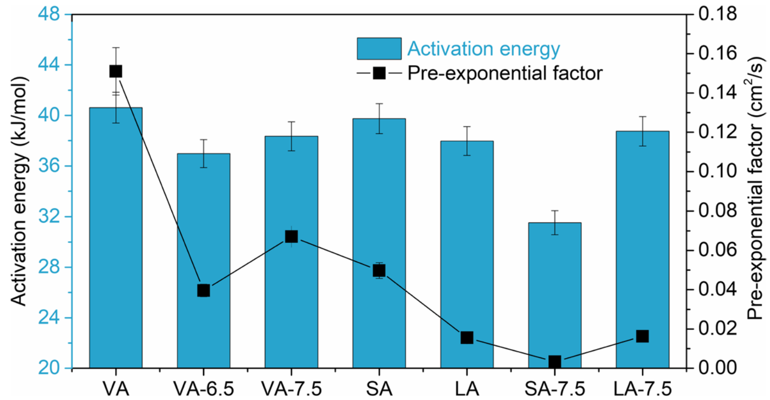

Fig. 21 Activation Energy and Pre-Exponential Factor of the Asphalt Models

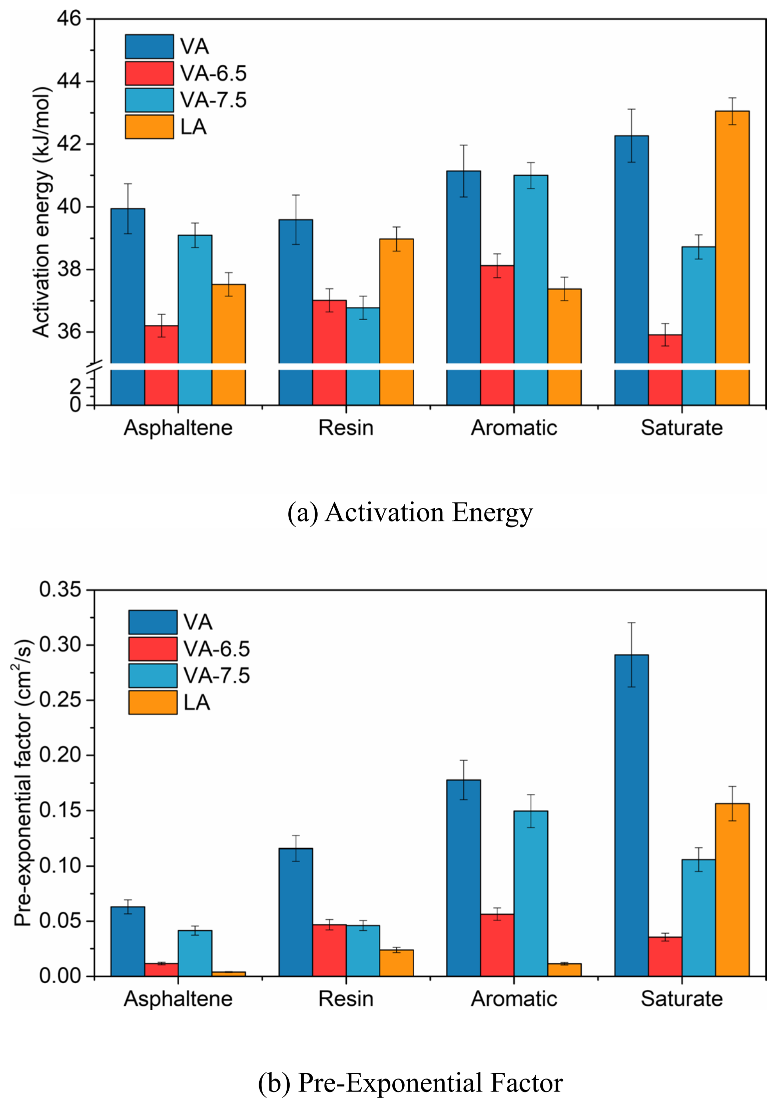

Fig. 22 Self-Healing Parameters of SARA Components in Asphalt Models: (**a**) Activation Energy, and (**b**) Pre-Exponential Factor

Table 3 Relationship between the Diffusion Coefficient of the SARA Components and System Temperatures

Models	Fraction	Fitting formula of lnD and 1/T	R^2
VA	Asphaltene	lnD = − 4804.50/T-2.764	0.9749
	Resin	lnD = − 4761.81/T-2.156	0.9635
	Aromaitc	lnD = − 4947.99/T-1.727	0.9804
	Saturate	lnD = − 5083.78/T-1.234	0.9090
VA-6.5	Asphaltene	lnD = − 4354.71/T-4.451	0.9585
	Resin	lnD = − 4451.96/T-3.060	0.9870
	Aromaitc	lnD = − 4585.19/T-2.874	0.9543
	Saturate	lnD = − 4319.64/T-3.336	0.9825
VA-7.5	Asphaltene	lnD = − 4701.88/T-3.182	0.9613
	Resin	lnD = − 4423.44/T-3.078	0.9762
	Aromaitc	lnD = − 4932.21/T-1.900	0.9890
	Saturate	lnD = − 4657.41/T-2.246	0.9868
LA	Asphaltene	lnD = − 4513.34/T-5.544	0.9856
	Resin	lnD = − 4687.66/T-3.735	0.9493
	Aromaitc	lnD = − 4496.13/T-4.473	0.9696
	Saturate	lnD = − 5178.10/T-1.856	0.9552

be found that VA-7.5 has the lower activation energy barrier and, thus, stronger instantaneous self-healing ability. This is consistent with the expected results.

Figure 22 shows the comparison of activation energy and the pre-exponential factor of each SARA component for four different asphalt binders. Table 3 shows the relationship between the diffusion coefficient of asphalt four components and temperature. From Fig. 22(a), it can be found that the activation energy of each component molecule of VA-6.5 and VA-7.5 is smaller than that of each component of VA. The activation energy for each component of LA is less than the activation energy of each VA component except the saturate component. This means that the addition of nano-SiO_2 can reduce the activation energy for each component of asphalt. The decrease in activation energy of the asphaltene, resin, and aromatic components of the long-term aged asphalt may be related to the oxidation of the molecules (saturate components are not subject to the oxidative aging). It can be seen from Fig. 22(b) that the pre-exponential factor of each VA component is higher than those of the other three asphalt. The pre-exponential factor for each component of VA-6.5 and VA-7.5 is higher than LA except for saturate component. This indicates that the instantaneous self-healing ability of the virgin asphalt is more robust than that of nano-SiO_2 modified asphalt and long-term aged asphalt. The instantaneous healing ability of nano-SiO_2 modified asphalt is more potent than that of long-term aged asphalt.

Moreover, for virgin asphalt, the activation energy of resin is the lowest, followed by asphaltene, aromatic, and saturate. Nevertheless, the pre-exponential factor order of the four components of virgin asphalt is asphaltene, resin, aromatic, and saturate in ascending order. It can be found that saturate and aromatic components mainly provide the instantaneous self-healing capacity of asphalt. After the addition of nano-SiO_2, the activation energy and factors of the 4-components of asphalt have changed. Therefore, the self-healing ability of the virgin asphalt can be improved by adding additives to change the activation energy and pre-exponential factor of the SARA components of asphalt material.

Figure 23 shows the comparison of 12 different molecules activation energy and pre-exponential factor of the virgin asphalt, long-term aged asphalt, and nano-SiO_2 modified asphalt. The activation energy of 12 molecules of VA, LA, and VA-7.5 is around 40 kJ/mol. The difference in activation energy between 12 molecules in VA and VA-7.5 is smaller, while the difference in activation energy between 12 molecules in LA is significant. This means that the colloidal structure of long-term aged asphalt may be more unstable. For the virgin asphalt model, the molecule with the largest pre-exponential factor is Re2. However, for long-term aged asphalt and nano-SiO_2 modified asphalt, the molecule with the largest pre-exponential factor is Sa1. In all three asphalt models, one molecule has a significantly higher pre-exponential factor than other molecules, and other molecules are relatively close. Therefore, it is possible to enhance the self-healing ability of asphalt by adding additives to make the difference in the activation energy of each molecule in the system smaller and increase the pre-exponential factor of a molecule.

Conclusions and outlook

This study provides a comprehensive understanding of the effect of nano-SiO_2 on the self-healing behavior of asphalt via the MD simulations from the nanoscale. The main conclusions can be drawn as follows:

(1) The self-healing process of asphalt nano-crack involves two phases, the typical artificial nano-crack healing stage, and the actual self-healing stage. The actual self-healing stage is characterized by a stable density curve and is close to the original asphalt density.
(2) Nano-SiO_2 can enhance the self-healing ability of asphalt, while oxidative aging harms the self-healing of asphalt. With the addition of nano-SiO_2 modifier, the diffusion coefficient of asphaltene reduces if compared to the virgin asphalt. Nano-SiO_2 has a significant enhancement effect on the diffusion rates of saturate, aromatic, and resin, whereas the diffusion coefficient of nano-SiO_2 is lower than the

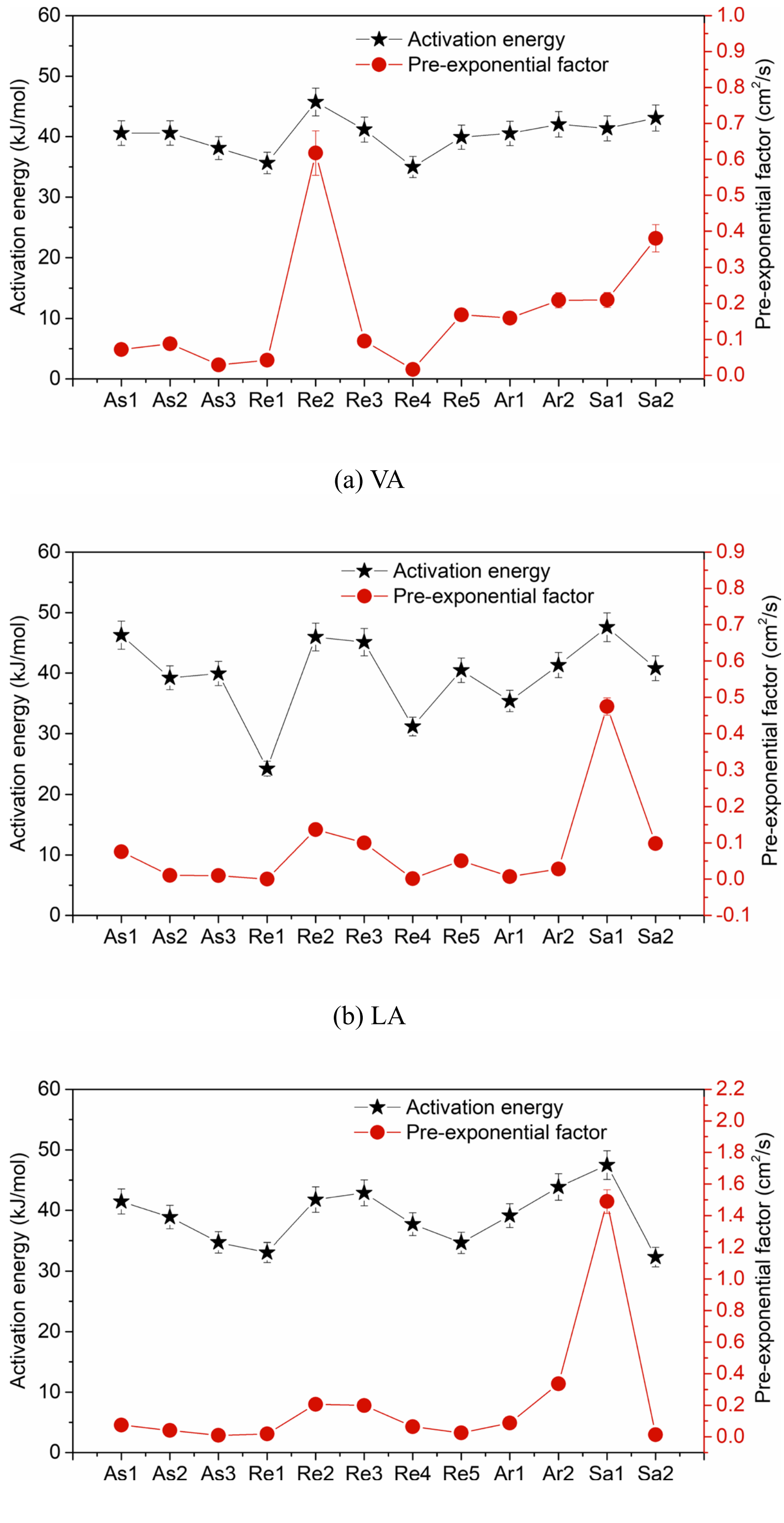

Fig. 23 Activation Energy and Pre-Exponential Factor of the Molecules in Asphalt Models: (**a**) VA, (**b**) LA, and (**c**) VA-7.5

other 4-components. Therefore, the self-healing capability of asphalt may be mainly determined by the diffusion of light components such as saturate, while nano-SiO_2 only plays an inducing role.

(3) Molecules with aromatic structures without alkyl side chains (Re1) and molecules with structures with longer alkyl chains (Ar1, Sa2, and Re5) may diffuse more easily; molecules with complex aromatic structures and more short alkyl side chains (As1) may be more difficult to diffuse. Nano-SiO_2 mainly improves the self-healing ability of the asphalt by enhancing the diffusion rate of molecules with aromatic structures without alkyl side chains and molecules with structures with longer alkyl chains.

(4) Nano-SiO_2 modified asphalt has a low activation energy barrier compared with virgin asphalt, although the instantaneous self-healing ability is weak. Simultaneously, nano-SiO_2 modified asphalt has a more significant diffusion coefficient; thus, it is believed that nano-SiO_2 can effectively improve the self-healing properties of asphalt if the temperature is higher than the glass transition temperature. As the degree of oxidative aging of asphalt increases, the instantaneous self-healing ability of asphalt weakens. Saturate and aromatic mainly provide the instantaneous self-healing capacity of asphalt.

(5) The addition of nano-SiO_2 can reduce the activation energy for each component of asphalt. The decrease in activation energy of the asphaltene, resin, and aromatic components of the long-term aged asphalt may be related to the oxidation of the molecules (saturate components are not subject to the oxidative aging).

The current study findings provide a fundamental understanding of the self-healing behavior and mechanism of nano-SiO_2 in asphalt from the perspective of molecules. The research opens new directions for further study on the effect of other environmental factors (such as moisture) on the self-healing behavior of asphalt from the nanoscale level.

Authors' contributions

ZL collected and synthesized references, conducted simulation, drafted and wrote the manuscript. XT proposed the simulation program. NG, YD and WM analyzed the simulation data. LY developed the research plan, reviewed and edited the manuscript. FX initiated the project and conceptualization. Both authors read and approved the final manuscript.

Funding

The authors acknowledge the financial support of Hunan Provincial Natural Science Foundation of China (2019JJ50622) and the Fundamental Research Funds for the Central Universities (2020kfyXJJS127).

Availability of data and materials

The datasets used and/or analyzed during the current study are available from the corresponding author on reasonable request.

Declarations

Consent for publication

Not applicable.

Competing interests

The authors declare that they have no competing interests.

Received: 3 December 2021 Accepted: 8 February 2022
Published online: 03 March 2022

References

1. Man J, Yan K, Miao Y, Liu Y, Yang X, Diab A, You L (2021) 3D spectral element model with a space-decoupling technique for the response of transversely isotropic pavements to moving vehicular loading. Road Mater Pavement Des (PRINT-IN-AHEAD):1–25
2. Polaczyk P, Huang B, Shu X, Gong H (2019) Investigation into locking point of asphalt mixtures utilizing Superpave and Marshall compactors. J Mater Civil Eng 31:4019188
3. Raab C, Camargo I, Partl MN (2017) Ageing and performance of warm mix asphalt pavements. J Traffic Trans Eng(English Edition) 4:388–394
4. Zhang E, Qi X, Shan L, Li D (2021) Investigation of rheological properties of asphalt emulsions. J Infrastruct Preserv Resilience 2:22
5. Fakhri M, Bahmai BB, Javadi S, Sharafi M (2020) An evaluation of the mechanical and self-healing properties of warm mix asphalt containing scrap metal additives. J Clean Prod 253:119963
6. You L, Jin D, Guo S, Wang J, Dai Q, You Z (2021) Leaching evaluation and performance assessments of asphalt mixtures with recycled cathode ray tube glass: a preliminary study. J Clean Prod 279:123716
7. Li R, Xiao F, Amirkhanian S, You Z, Huang J (2017) Developments of nano materials and technologies on asphalt materials – a review. Constr Build Mater 143:633–648
8. Ali SIA, Ismail A, Karim MR, Yusoff NIM, Al-Mansob RA, Aburkaba E (2017) Performance evaluation of Al2O3 nanoparticle-modified asphalt binder. Road Mater Pavement 18:1251–1268
9. Moreno-Navarro F, Sol-Sánchez M, Gámiz F, Rubio-Gámez MC (2018) Mechanical and thermal properties of graphene modified asphalt binders. Constr Build Mater 180:265–274
10. Kuntikana G, Singh D (2017) Contemporary issues related to utilization of industrial byproducts. Adv Civil Eng Mater 6:444–479
11. Mamun AA, Arifuzzaman M (2018) Nano-scale moisture damage evaluation of carbon nanotube-modified asphalt. Constr Build Mater 193:268–275
12. Guo S, Dai Q, Wang Z, Yao H (2017) Rapid microwave irradiation synthesis of carbon nanotubes on graphite surface and its application on asphalt reinforcement. Compos Part B 124:134–143
13. Mousavi SE, Karamvand A (2017) Assessment of strength development in stabilized soil with CBR PLUS and silica sand. J Traffic Trans Eng 4:412–421
14. Crucho JML, Neves JMCD, Capitão SD, Picado-Santos LGD (2018) Mechanical performance of asphalt concrete modified with nanoparticles: Nanosilica, zero-valent iron and nanoclay. Constr Build Mater 181:309–318
15. Ortega FJ, Navarro FJ, García-Morales M, McNally T (2015) Thermo-mechanical behaviour and structure of novel bitumen/nanoclay/MDI composites. Compos Part B 76:192–200
16. Karnati SR, Oldham D, Fini EH, Zhang L (2019) Surface functionalization of silica nanoparticles to enhance aging resistance of asphalt binder. Constr Build Mater 211:1065–1072
17. Yusoff NIM, Breem AAS, Alattug HNM, Hamim A, Ahmad J (2014) The effects of moisture susceptibility and ageing conditions on nano-silica/polymer-modified asphalt mixtures. Constr Build Mater 72:139–147
18. Ho C, Martin Linares C, Shan J, Almonnieay A (2017) Material testing apparatus and procedures for evaluating freeze-thaw resistance of asphalt concrete mixtures. Adv Civil Eng Mater 6:429–443

19. Nazari H, Naderi K, Moghadas Nejad F (2018) Improving aging resistance and fatigue performance of asphalt binders using inorganic nanoparticles. Constr Build Mater 170:591–602
20. Valizadeh M, Janalizadeh Choobbasti A (2020) Evaluation of nano-graphene effect on mechanical behavior of clayey sand with microstructural and self-healing approach. J Adhes Sci Technol 34:299–318
21. HasaniNasab S, Arast M, Zahedi M (2019) Investigating the healing capability of asphalt modified with nano-zycotherm and Forta fibers. Case Stud Constr Mater 11:e235
22. Amin GM, Esmail A (2017) Application of nano silica to improve self-healing of asphalt mixes. J Cent South Univ 24:1019–1026
23. Kie Badroodi S, Reza Keymanesh M, Shafabakhsh G (2020) Experimental investigation of the fatigue phenomenon in nano silica-modified warm mix asphalt containing recycled asphalt considering self-healing behavior. Constr Build Mater 246:117558
24. Ganjei MA, Aflaki E (2019) Application of nano-silica and styrene-butadiene-styrene to improve asphalt mixture self healing. Int J Pavement Eng 20:89–99
25. Hosseinnezhad S, Shakiba S, Mousavi M, Louie SM, Karnati SR, Fini EH (2019) Multiscale evaluation of moisture susceptibility of biomodified bitumen. ACS Appl Bio Mater 2:5779–5789
26. Mousavi M, Oldham DJ, Hosseinnezhad S, Fini EH (2019) Multiscale evaluation of synergistic and antagonistic interactions between bitumen modifiers. ACS Sustain Chem Eng 7:15568–15577
27. Mousavi M, Fini E (2020) Silanization mechanism of silica nanoparticles in bitumen using 3-Aminopropyl Triethoxysilane (APTES) and 3-Glycidyloxypropyl Trimethoxysilane (GPTMS). ACS Sustain Chem Eng 8:3231–3240
28. Xu M, Yi J, Feng D, Huang Y, Wang D (2016) Analysis of adhesive characteristics of asphalt based on atomic force microscopy and molecular dynamics simulation. ACS Appl Mater Inter 8:12393–12403
29. Samieadel A, Høgsaa B, Fini EH (2019) Examining the implications of wax-based additives on the sustainability of construction practices: multiscale characterization of wax-doped aged asphalt binder. ACS Sustain Chem Eng 7:2943–2954
30. Long Z, Zhou S, Jiang S, Ma W, Ding Y, You L, Tang X, Xu F (2021) Revealing compatibility mechanism of nanosilica in asphalt through molecular dynamics simulation. J Mol Model 27:81
31. Tang J, Wang H (2022) Coarse grained modeling of nanostructure and asphaltene aggregation in asphalt binder using dissipative particle dynamics. Constr Build Mater 314:125605
32. Fini EH, Hung AM, Roy A (2019) Active mineral fillers arrest migrations of alkane acids to the Interface of bitumen and siliceous surfaces. ACS Sustain Chem Eng 7:10340–10348
33. Chen Z, Pei J, Li R, Xiao F (2018) Performance characteristics of asphalt materials based on molecular dynamics simulation – a review. Constr Build Mater 189:695–710
34. Yao H, Liu J, Xu M, Ji J, Dai Q, You Z (2022) Discussion on molecular dynamics (MD) simulations of the asphalt materials. Adv Colloid Interfac 299:102565
35. Khabaz F, Khare R (2015) Glass transition and molecular mobility in styrene–butadiene rubber modified asphalt. J Phys Chem B 119:14261–14269
36. Yao H, Dai Q, You Z (2016) Molecular dynamics simulation of physicochemical properties of the asphalt model. FUEL 164:83–93
37. Su M, Si C, Zhang Z, Zhang H (2020) Molecular dynamics study on influence of Nano-ZnO/SBS on physical properties and molecular structure of asphalt binder. FUEL 263:116777
38. Pan J, Tarefder RA (2016) Investigation of asphalt aging behaviour due to oxidation using molecular dynamics simulation. Mol Simulat 42:667–678
39. Xu G, Wang H (2017) Molecular dynamics study of oxidative aging effect on asphalt binder properties. Fuel 188:1–10
40. Fallah F, Khabaz F, Kim Y, Kommidi SR, Haghshenas HF (2019) Molecular dynamics modeling and simulation of bituminous binder chemical aging due to variation of oxidation level and saturate-aromatic-resin-asphaltene fraction. Fuel 237:71–80
41. Yu R, Wang Q, Wang W, Xiao Y, Wang Z, Zhou X, Zhang X, Zhu X, Fang C (2021) Polyurethane/graphene oxide nanocomposite and its modified asphalt binder: preparation, properties and molecular dynamics simulation. Mater Design 209:109994
42. Su M, Zhou J, Lu J, Chen W, Zhang H (2022) Using molecular dynamics and experiments to investigate the morphology and micro-structure of SBS modified asphalt binder. Mater Today Commun 30:103082
43. Cui B, Wang H (2022) Molecular interaction of asphalt-aggregate interface modified by silane coupling agents at dry and wet conditions. Appl Surf Sci 572:151365
44. Cui W, Huang W, Hassan HMZ, Cai X, Wu K (2022) Study on the interfacial contact behavior of carbon nanotubes and asphalt binders and adhesion energy of modified asphalt on aggregate surface by using molecular dynamics simulation. Constr Build Mater 316:125849
45. Ding Y, Huang B, Shu X, Zhang Y, Woods ME (2016) Use of molecular dynamics to investigate diffusion between virgin and aged asphalt binders. Fuel 174:267–273
46. Huang M, Zhang H, Gao Y, Wang L (2019) Study of diffusion characteristics of asphalt–aggregate interface with molecular dynamics simulation. Int J Pavement Eng:1–12
47. Xu M, Yi J, Feng D, Huang Y (2019) Diffusion characteristics of asphalt rejuvenators based on molecular dynamics simulation. Int J Pavement Eng 20:615–627
48. Xu G, Wang H (2016) Molecular dynamics study of interfacial mechanical behavior between asphalt binder and mineral aggregate. Constr Build Mater 121:246–254
49. Dong Z, Liu Z, Wang P, Gong X (2017) Nanostructure characterization of asphalt-aggregate interface through molecular dynamics simulation and atomic force microscopy. Fuel 189:155–163
50. Gao Y, Zhang Y, Yang Y, Zhang J, Gu F (2019) Molecular dynamics investigation of interfacial adhesion between oxidised bitumen and mineral surfaces. Appl Surf Sci 479:449–462
51. Long Z, You L, Tang X, Ma W, Ding Y, Xu F (2020) Analysis of interfacial adhesion properties of nano-silica modified asphalt mixtures using molecular dynamics simulation. Constr Build Mater 255:119354
52. Shen S, Lu X, Liu L, Zhang C (2016) Investigation of the influence of crack width on healing properties of asphalt binders at multi-scale levels. Constr Build Mater 126:197–205
53. Sun D, Lin T, Zhu X, Tian Y, Liu F (2016) Indices for self-healing performance assessments based on molecular dynamics simulation of asphalt binders. Comp Mater Sci 114:86–93
54. He L, Zheng Y, Alexiadis A, Cannone Falchetto A, Li G, Valentin J, Van den Bergh W, Emmanuilovich Vasiliev Y, Kowalski KJ, Grenfell J (2021) Research on the self-healing behavior of asphalt mixed with healing agents based on molecular dynamics method. Constr Build Mater 295:123430
55. Tian Y, Zheng M, Liu Y, Zhang J, Ma S, Jin J (2021) Analysis of behavior and mechanism of repairing agent of microcapsule in asphalt micro crack based on molecular dynamics simulation. Constr Build Mater 305:124791
56. Sun D, Sun G, Zhu X, Ye F, Xu J (2018) Intrinsic temperature sensitive self-healing character of asphalt binders based on molecular dynamics simulations. Fuel 211:609–620
57. He L, Li G, Lv S, Gao J, Kowalski KJ, Valentin J, Alexiadis A (2020) Self-healing behavior of asphalt system based on molecular dynamics simulation. Constr Build Mater 254:119225
58. Yu T, Zhang H, Wang Y (2020) Multi-gradient analysis of temperature self-healing of asphalt nano-cracks based on molecular simulation. Constr Build Mater 250:118859
59. Sun H (1998) COMPASS: an ab initio force-field optimized for condensed-phase ApplicationsOverview with details on alkane and benzene compounds. J Phys Chem B 102:7338–7364
60. Nosé S (1984) A unified formulation of the constant temperature molecular dynamics methods. J Chem Phys 81:511–519
61. Hoover WG (1985) Canonical dynamics: equilibrium phase-space distributions, physical review. Gen Phys 31:1695–1697
62. Li DD, Greenfield ML (2014) Chemical compositions of improved model asphalt systems for molecular simulations. Fuel 115:347–356
63. Qu X, Liu Q, Guo M, Wang D, Oeser M (2018) Study on the effect of aging on physical properties of asphalt binder from a microscale perspective. Constr Build Mater 187:718–729
64. Jones DR (1993) SHRP materials reference library: asphalt cements: a concise data compilation. National Research Council, Washington, DC
65. DJ MGE (2014) Statistical mechanics of nonequilibrium liquids. Cambridge University, New York

66. Daivis PJ, Todd BD (2006) A simple, direct derivation and proof of the validity of the SLLOD equations of motion for generalized homogeneous flows. J Chem Phys 124:194103
67. Han J, Gee RH, Boyd RH (1994) Glass transition temperatures of polymers from molecular dynamics simulations. Macromolecules 27:7781–7784
68. Laidler KJ (1984) The development of the Arrhenius equation. J Chem Educ 61:494
69. Robertson RE, Branthaver JF, Harnsberger PM, Petersen JC, Dorrence SM, McKay JF, Turner TF, Pauli AT (2001) Fundamental Properties of Asphalt and Modified Asphalts, vol. I, Interpretive Report
70. Tabatabaee HA, Velasquez R, Bahia HU (2012) Predicting low temperature physical hardening in asphalt binders. Constr Build Mater 34:162–169
71. Daly WH, Negulescu II, Glover I (2010) A comparative analysis of modified binders: original asphalt and material extracted from existing pavement, l. Louisiana State University Baton Rouge (Ed.). L. Louisiana State University Baton Rouge, Louisiana
72. García Á (2012) Self-healing of open cracks in asphalt mastic. Fuel 93:264–272

Publisher's Note

Springer Nature remains neutral with regard to jurisdictional claims in published maps and institutional affiliations.